Accuracies of field CO_2−H_2O data from open-path eddy-covariance flux systems: Assessment based on atmospheric physics and biological environment

Xinhua Zhou[1,2], Bai Yang[2], Tian Gao[1,3], Ning Zheng[1,4], Yanlei Li[1,2], Fengyuan Yu[1,3], Tala Awada[5], Jiaojun Zhu[1,3]

[1] Ker Research and Development, CAS Key Laboratory of Forest Ecology and Management, Institute of Applied Ecology, Chinese Academy of Sciences, Shenyang 110015, China
[2] Campbell Scientific Inc., Logan, UT 84321, USA
[3] Qingyuan Forest CERN, National Observation and Research Station, Liaoning Province, Shenyang 110015, China
[4] Beijing Servirst Technology Limited, Beijing 102299, China
[5] School of Natural Resources, University of Nebraska, Lincoln, NE 68583, USA

Correspondence to: Tian Gao (tiangao@iae.ac.cn) and Ning Zheng (ning.zheng@servirst.com)

Abstract. Ecosystem CO_2−H_2O data measured by infrared gas analyzers in open-path eddy-covariance (OPEC) systems have numerous applications, such as estimations of CO_2 and H_2O fluxes in the atmospheric boundary layer. To assess the applicability of these estimations, data uncertainties from infrared gas analyzer measurements are needed. The uncertainties are sourced from infrared analyzers in zero drift, gain drift, cross-sensitivity, and precision variability. The sourced uncertainties are individually specified for analyzer performance, but no methodology exists to comprehend these individual uncertainties into an integrated error for the specification of an overall accuracy, which is ultimately needed. Using the methodology for close-path eddy-covariance systems, this accuracy for OPEC systems is determined from all individual uncertainties via an accuracy model and further formulated into CO_2 and H_2O accuracy equations. Based on atmospheric physics and the biological environment, for EC150 infrared CO_2−H_2O analyzers, these equations are used to evaluate CO_2 accuracy (± 1.21 mgCO_2 m^{-3}, relatively $\pm 0.19\%$) and H_2O accuracy (± 0.10 gH_2O m^{-3}, relatively $\pm 0.18\%$ in saturated air at 35 °C and 101.325 kPa). Cross-sensitivity and precision variability are minor, although unavoidable, uncertainties. Zero drifts and gain drifts are major uncertainties but are adjustable via corresponding zero and span procedures during field maintenance. The equations provide rationales to assess and guide the procedures. For a background concentration of atmospheric CO_2, CO_2 zero and span procedures can narrow the CO_2 accuracy range by 40%, from ± 1.21 to ± 0.72 mgCO_2 m^{-3}. In hot and humid weather, H_2O gain drift potentially adds more to H_2O measurement uncertainty, which requires more attention. If H_2O zero and span procedures can be performed practically from 5 to 35 ºC, the H_2O accuracy can be improved by 30% at minimum, from ± 0.10 to ± 0.07 gH_2O m^{-3}. The H_2O span procedure is impractical under freezing conditions but can be neglected because of its trivial contributions to the overall uncertainty. However, the zero procedure for H_2O, along with CO_2, is imperative as an operational and efficient option under these conditions to minimize H_2O measurement uncertainty.

1 Introduction

35   Open-path eddy-covariance (OPEC) systems are used mostly to measure boundary-layer CO_2, H_2O, heat, and momentum fluxes between ecosystems and the atmosphere (Lee and Massman, 2011). For flux measurements, an OPEC system is equipped with a fast-response three-dimensional (3-D) sonic anemometer, to measure 3-D wind velocities and sonic temperature (T_s), and a fast-response infrared $CO_2−H_2O$ analyzer (hereafter referred to as an infrared analyzer or analyzer) to measure CO_2 and H_2O concentrations or densities (Fig. 1). In this system, the analyzer is adjacent to the sonic measurement

40   volume. Both anemometer and analyzer together provide synchronized high-frequency (e.g., 10 to 20 Hz) measurements, which are used to compute the fluxes at a location represented by the measurement volume (Aubinet et al., 2012). Given that the measurement conditions, which are spatially homogenous in flux sources/sinks and temporally steady in turbulent flows without advection, satisfy the underlying theory for eddy-covariance flux techniques (Katul et al., 2004; Finnigan, 2008), the quality of each flux data primarily depends on the field measurement exactness of variables, such as CO_2, H_2O, T_s, and 3-D

45   wind, at the sensor sensing scales (Foken et al., 2012; Richardson et al., 2012), although this quality can also be degraded by other biases if not fully corrected. In an OPEC system, other biases are commonly sourced from the tilt of vertical axis of the sonic anemometer away from the natural wind (Kaimal and Haugen, 1969), the spatial separation between the anemometer and the analyzer (Laubach and McNaughton, 1998), the line and/or volume averaging in measurements (Wyngaard, 1971; Andreas, 1981), the response delay of sensors to fluctuations in measured variables (Horst, 2000), the air density fluctuations

50   due to heat and water fluxes (Webb et al., 1980), and the filtering in data processing (Rannik and Vesala, 1999). These biases are correctable through coordinate rotation corrections for the tilt (Tanner and Thurtell, 1960; Wilczak, 2001), covariance lag maximization for the separation (Moncrieff et al., 1997; Ibrom et al., 2007), low- and high-frequency corrections for the data filtering, line and/or volume averaging, and response delay (Moore, 1986; Lenschow et al., 1994; Massman, 2000; van Dijk, 2002), and WPL corrections for the air density fluctuations (Webb et al., 1980). Even though these corrections are thorough

55   for corresponding biases, errors in the ultimate flux data still exist due to uncertainties related to measurement exactness of the sensor sensing scales (Fratini et al., 2014; Zhou et al., 2018). These uncertainties are not only unavoidable because of actual or apparent instrumental drifts due to the thermal sensitivity of sensor path lengths, long-term aging of sensor detection components, and unexpected factors in field operations (Fratini et al., 2014), but they are also not mathematically correctable because their sign and magnitude are unknown (Richardson et al., 2012). The overall measurement exactness

60   related to these uncertainties would be a valuable addition to flux data analysis (Goulden et al., 1996; Anthoni et al., 2004).
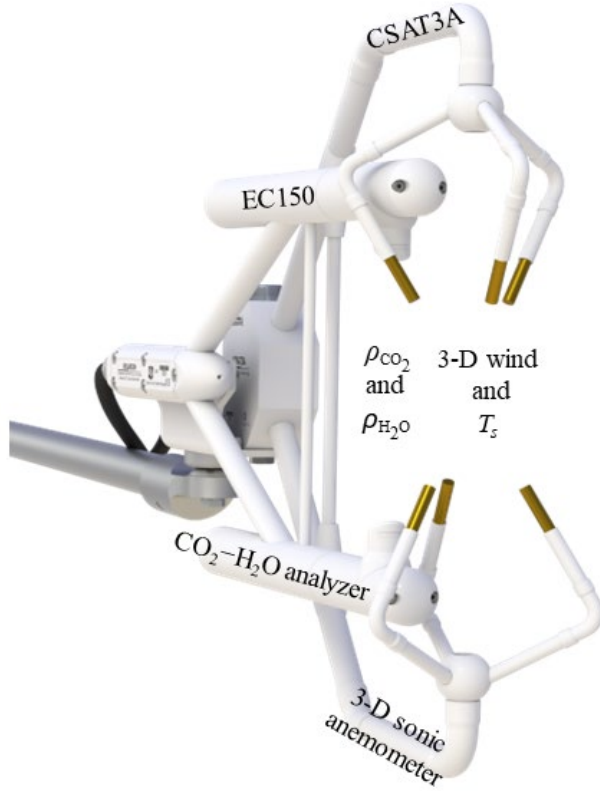
Figure 1. Integration of a CSAT3A sonic anemometer for three-dimensional (3-D) wind velocities and sonic temperature (T_s) and an EC150 infrared CO_2–H_2O analyzer for CO_2 density (ρ_{CO_2}) and H_2O density (ρ_{H_2O}) in an open-path eddy-covariance flux system (Campbell Scientific Inc., UT, USA).

In addition to flux computations, the data for individual variables from these field measurements can be important in numerous applications. Knowledge of measurement exactness is also required for accurate assessment of data applicability (Csavina et al., 2017; Hill et al., 2017). The infrared analyzer in an OPEC system output CO_2 density (ρ_{CO_2} in mgCO_2 m^{-3}) and H_2O density (ρ_{H_2O} in gH_2O m^{-3}). For instance, ρ_{H_2O}, along with T_s and atmospheric pressure (P), can be used to derive ambient air temperature (T_a) (Swiatek, 2018). In this case, given an exact equation of T_a in terms of the three independent variables ρ_{H_2O}, T_s, and P, the applicability of this equation to the OPEC systems for T_a depends wholly on the measurement exactness of the three independent variables. The higher the degree of exactness, the less uncertain the T_a. The assessment on the applicability necessitates the knowledge of the measurement exactness. In reality, to the best of our knowledge, neither the overal measurement exactness of ρ_{H_2O} from infrared analyzers nor this exactness of T_s from sonic anemometers (personal commnication: Larry Jecobsen, 2022) is availble. This study defines and estimates the measurement exactness of ρ_{H_2O} including ρ_{CO_2} from infrared analyzers through cumulating the measurement uncertainties, which is not mathematically correctable.

3

As comprehensively reviewed by Richardson et al. (2012), numerous previous studies including Goulden et al. (1996), Lee et al. (199), Anthoni et al. (1999, 2004), and Flanagan and Johonson (2005) have quantified various sources of flux measurement uncertainties and have attempted to attach confidence intervals to the annual sums of net ecosystem exchange. These sources include measurement methods (e.g., sensor separation and site homogeneity (Munger et al., 2012)), data processing algorithms (e.g., data filtering (Rannik and Vesala, 1999) and data gap filling (Richardson and Hollinger, 2007)), measurement conditions (e.g., advection (Finnigan, 2008)), energy closure (Foken, 2008), and sensor body heating effect (Burba et al., 2008). Instead of quantifying the flux uncertainties, Foken et al. (2004, 2012) assessed the flux data into nine grades (1 to 9) based on steady state, turbulence conditions, and wind direction in the sonic anemometer coordinate system. The lower the grade, the less uncertainty; the higher grade, the more uncertainty. The grade matrix for flux data uncertainty (e.g., quality) has been adopted by AmeriFlux (2018). In other aspects to correct the measurement bias from infrared analyzers, Burba et al. (2008) developed the correction for a sensor body heating effect on CO_2 and H_2O fluxes, wheras Fratini et al. (2014) developed a method for correcting the raw high-frequency CO_2 and H_2O data using the zero and span coeffcients of an infrared gas analyzer that were acquired from the same conditions, but at the begnning and ending of a time period. The corrected data were used to re-estimate the fluxes. To the best of our knowledge, no study has addressed the uncorrectable, although preventable to some degree, overall uncertainties in CO_2 and H_2O data from infrared anlyzers, even though both overall uncertainties are fundamental for data analysis in applications (Richardson et al., 2012).

Although uncertainty sources in CO_2 and H_2O measurements, such as analyzer zero and gain drifts, analyzer background sensitivities, and measurement precision variability, are separately specified (LI−COR Biosciences, 2021b; Campbell Scientific Inc., 2021b), the specification for overall exactness of an individual field CO_2 or H_2O measurement is unavailable due to the absence of methodology to composite all of the specified measurement uncertainties into an integrated one. For any sensor, the measurement exactness depends on its performances as commonly specified in terms of accuracy, precision, and other uncertainty descriptors such as sensor drift. Conventionally, accuracy is defined as a systematic uncertainty, and precision is defined as a random measurement error (ISO, 2012, where ISO is the acronym of International Organization for Standardization). Other uncertainty descriptors are also defined for specific reliabilities in instrumental performance. For example, CO_2 zero drift is one of the descriptors specified for the performance of infrared analyzers in CO_2 measurements (Campbell Scientific Inc., 2021b). Both accuracy and precision are universally applicable to any sensor for the specification of its performance in measurement exactness. Other uncertainty descriptors are more sensor-specific (e.g., cross-sensitivity to CO_2/H_2O is used for infrared analyzers in OPEC and CPEC systems, where CPEC is an acronym for closed-path eddy-covariance).

Conventionally, sensor accuracy is the degree of closeness to which its measurements are to the true value in the measured variable; sensor precision, related to repeatability, is the degree to which repeated measurements under unchanged conditions produce the same values (Joint Committee for Guides in Metrology, 2008). Another definition advanced by the ISO (2012), revising the conventional definition of accuracy as trueness originally representing only systematic uncertainty,

specifies accuracy as a combination of both trueness and precision. An advantage of this definition for accuracy is the consolidation of all measurement uncertainties. According to this definition, the accuracy is the range of cumulative uncertainty from all sources in field measurements. For CPEC systems, Zhou et al. (2021) developed a method and derived a model to assess the accuracy of CO_2/H_2O mixing ratio measurements by infrared analyzers. Their model was further formulated as a set of equations to evaluate the defined accuracies for CO_2 and H2O mixing rato data from CPEC systems. Although the CPEC systems are very different from OPEC systems in their structural designs (e.g., measurements take place inside a closed cuvette *vs*. in an open space) and in output variables (e.g., CO_2/H_2O mixing ratio *vs*. CO_2/H_2O density), similarities exist between the two systems in measurement uncertainties as specified by their manufacturers (Campbell Scientific Inc., 2021a,; 2021b) because the infrared analyzers in both systems use the same physics theories and similar optical techinques for their measurements (LI−COR Biosciences, 2021a; 2021b). Accordingly, the method developed by Zhou et al. (2021) for CPEC systems can be reasonably applicable to their OPEC counterparts with rederivation of model and reformulation of equations. Following the methdology of Zhou et al. (2021) and using the specifications of EC150 infrared analyzers in OPEC systems as an example (Campbell Scientific Inc., 2021b), we derive the model and formulate equations to assess the accuracies of CO_2 and H_2O measurements by infrared analyzers in OPEC systems, discuss the usage of accuracies in flux analysis, data applications, and analyzer field maintenance, and ultimately provide a reference for the flux measurement community to specify the overall accuracy of field CO_2/H_2O measurements by infrared analyzers in OPEC systems.

2 Specification implications

An OPEC system for this study includes, but is not limited to, a CSAT3A sonic anemometer, and an EC150 infrared analyzer (Fig. 1). The system operates in a T_a range from –30 to 50 °C and in a P range from 70 to 106 kPa. Within these operational ranges, the specifications for CO_2 and H_2O measurements (Campbell Scientific Inc., 2021b) are given in Table 1.

Table 1. Measurement specifications for EC150 infrared CO_2-H_2O analyzers

	CO₂			H₂O			Note
	notation	value	Unit	notation	value	unit	
Calibration range		$0-1{,}553$	$mgCO_2\ m^{-3}$		$0-44$	$gH_2O\ m^{-3}$	For CO_2 up to 4,500 $mgCO_2\ m^{-3}$ if specially needed.
Zero drift	d_{cz}	±0.55	$mgCO_2\ m^{-3}$	d_{wz}	±0.04	$gH_2O\ m^{-3}$	Zero/gain drift is the possible maximum range within the system operational ranges in ambient air temperature (T_a) and atmospheric pressure. The actual drift depends more on T_a.
Gain drift	d_{cg}	$\pm0.10\%$ [a/] true ρ_{CO_2}	$mgCO_2\ m^{-3}$	d_{wg}	$\pm0.30\%$ [b/] true ρ_{H2O}	$gH_2O\ m^{-3}$	
Cross-sensitivity to H₂O	s_{H2O}	$\pm2.69\times10^{-7}$	$mgCO_2\ m^{-3}$ $(gH_2O\ m^{-3})^{-1}$		N/A		
Cross-sensitivity to CO₂		N/A		s_{CO2}	$\pm4.09\times10^{-5}$	$gH_2O\ m^{-3}$ $(mgCO_2\ m^{-3})^{-1}$	
Precision	σ_{CO2}	0.200	$mgCO_2\ m^{-3}$	σ_{H2O}	0.004	$gH_2O\ m^{-3}$	

[a] 0.10% is the CO_2 gain drift percentage denoted by δ_{CO2_g} in text, and ρ_{CO_2} is CO_2 density.

[b] 0.30% is the H_2O gain drift percentage denoted by δ_{H2O_g} in text, and ρ_{H2O} is H_2O density.

155   In Table 1, the top limit of 1,553 $mgCO_2\ m^{-3}$ in the calibration range for CO_2 density in dry air is more than double the atmospheric background CO_2 density of 760 $mgCO_2\ m^{-3}$, or 415 $\mu molCO_2\ mol^{-1}$, where mol is the unit for dry air, reported by Global Monitoring Laboratory (2021) with a T_a of 20 °C under a P of 101.325 kPa (i.e., normal temperature and pressure - Wright et al. (2003)). The top limit of 44 $gH_2O\ m^{-3}$ in the calibration range for H_2O density is equivalent to a 37 °C dew point, higher than the highest 35 °C dew point ever recorded under natural conditions on the Earth (National 160   Weather Service, 2021).

      The measurement uncertainties of infrared analyzers for CO_2 and H_2O in Table 1 are specified by individual uncertainty components along with their magnitudes: zero drift, gain drift, cross-sensitivity to CO_2/H_2O, and precision variability. Zero drift uncertainty is an analyzer non-zero response to zero air/gas (i.e., air/gas free of CO_2 and H_2O). Gain drift uncertainty is an analyzer trend-deviation response to measured gas species away from its true value in proportion 165   (Campbell Scientific Inc., 2021b). Cross-sensitivity is an analyzer background response to either CO_2 if H_2O is measured, or H_2O if CO_2 is measured. Precision variability is an analyzer random response to minor unexpected factors. For CO_2 and H_2O, respectively, these four components should be composited as a cumulative uncertainty to evaluate the accuracy that is ultimately needed in practice.

Precision variability is a random error, and the other specifications can be considered as trueness. Zero drifts are primarily impacted by T_a, and so are gain drifts. Additionally, each gain drift is also positively proportional to the true magnitude of CO_2/H_2O density (i.e., true ρ_{CO_2} or true ρ_{H_2O}) under measurements. Lastly, cross-sensitivity to H_2O/CO_2 is related to the background amount of H_2O/CO_2 as indicated by its units, $mgCO_2\,m^{-3}\,(gH_2O\,m^{-3})^{-1}$ for CO_2 measurements, and $gH_2O\,m^{-3}\,(mgCO_2\,m^{-3})^{-1}$ for H_2O measurements.

Accordingly, beyond statistical analysis, the accuracy of CO_2/H_2O measurements should be evaluated over a T_a range of -30 to $50\ ^\circ C$, a ρ_{H_2O} range of up to $44\ gH_2O\,m^{-3}$, and a ρ_{CO_2} range of up to $1{,}553\ mgCO_2\,m^{-3}$.

3 Accuracy model

The measurement accuracy of infrared analyzers is the possible maximum range of cumulative measurement uncertainty from the four uncertainty components as specified in Table 1: zero drift, gain drift, cross-sensitivity, and precision variability. The four uncertainties interactionally or independently contribute to the overall uncertainty of a measured value. Given the true α density ($\rho_{\alpha T}$, where subscript α can be either CO_2 or H_2O) and measured α density (ρ_α), the difference between the true and measured α densities ($\Delta\rho_\alpha$) is given by

$$\Delta\rho_\alpha = \rho_\alpha - \rho_{\alpha T}. \tag{1}$$

The analyzer overestimates the true value if $\Delta\rho_\alpha > 0$, exactly estimates the true value if $\Delta\rho_\alpha = 0$, and underestimates the true value if $\Delta\rho_\alpha < 0$. The measurement accuracy is the maximum range of $\Delta\rho_\alpha$ (i.e., an accuracy range). According to the analyses of Zhou et al. (2021) for CPEC infrared analyzers, as mathematically shown in Apendix A, this range is interactionally contributed by the zero drift uncertainty $(\Delta\rho_\alpha^z)$, gain drift uncertainty $(\Delta\rho_\alpha^g)$, and cross-sensitivity uncertainty $(\Delta\rho_\alpha^s)$ along with an independent additon from the precision uncertainty $(\Delta\rho_\alpha^s)$. However, any interactional contribution from a pair of uncertainties is three orders smaller in magnitude than each individual contribution in the pair. The contribution to the accuracy range due to interactions can be reasonably neglected. Therefore, the accuracy range can be simply modeled as a sum of the four components uncertainties in their absolute values. From Eq. (A7) in Appendix A, the measurement accuracy of α density from OPEC systems by infrared analyzers is defined in an accuracy model as

$$\Delta\rho_\alpha \equiv \pm\left(\left|\Delta\rho_\alpha^z\right| + \left|\Delta\rho_\alpha^g\right| + \left|\Delta\rho_\alpha^s\right| + \left|\Delta\rho_\alpha^p\right|\right). \tag{2}$$

Assessment on the accuracy of field CO_2 or H_2O measurements is, by use of known and/or estimable variables, to formulate and evaluate the four terms on the right side of this accuracy model.

4 Accuracy of CO_2 density measurements

Based on accuracy Model (2), we define the accuracy of field CO_2 measurements from OPEC systems by infrared analyzers ($\Delta\rho_{CO_2}$) as

$$\Delta\rho_{CO_2} \equiv \pm\left(\left|\Delta\rho_{CO_2}^z\right| + \left|\Delta\rho_{CO_2}^g\right| + \left|\Delta\rho_{CO_2}^s\right| + \left|\Delta\rho_{CO_2}^p\right|\right), \tag{3}$$

where $\Delta\rho_{CO_2}^z$ is CO$_2$ zero drift uncertainty, $\Delta\rho_{CO_2}^g$ is CO$_2$ gain drift uncertainty, $\Delta\rho_{CO_2}^s$ is cross-sensitivity-to-H$_2$O uncertainty,

200 and $\Delta\rho_{CO_2}^p$ is CO$_2$ precision uncertainty.

CO$_2$ precision (σ_{CO_2}) is the standard deviation of ρ_{CO_2} random errors among repeated measurements under the same conditions (Joint Committee for Guides in Metrology, 2008). The random errors generally have a normal distribution in statistics (Hoel, 1984). Therefore, using this deviation, the precision uncertainty for an individual CO$_2$ measurement at a 95% confidence interval (P-value of 0.05) can be statistically formulated as

205 $$\Delta\rho_{CO_2}^p = \pm 1.96 \times \sigma_{CO_2}. \tag{4}$$

The other uncertainties, due to CO$_2$ zero drift, CO$_2$ gain drift, and cross-sensitivity-to-H$_2$O, are caused by the inability of the working equation inside an infrared analyzer to be adapted to the changes in its internal and ambient environmental conditions, such as internal housing CO$_2$ and/or H$_2$O levels and ambient air temperature. From the derivations in the Theory and operation section in LI−COR Biosciences (2001, 2021a, 2021b), a general model of the

210 working equation for ρ_{CO_2} is given by

$$\rho_{CO_2} = P\sum_{i=1}^{5} a_{ci}\left\{1 - \left[\frac{A_c}{A_{cs}} + S_w\left(1 - \frac{A_w}{A_{ws}}\right)\right]Z_c\right\}^i \left\{\frac{G_c}{P}\right\}^i, \tag{5}$$

where subscripts c and w indicate CO$_2$ and H$_2$O, respectively; a_{ci} (i = 1, 2, 3, 4, or 5) is a coefficient of the five-order polynomial for the terms inside curly brackets; A_{cs} and A_{ws} are the power values of analyzer source lights at the chosen wavelengths for CO$_2$ and H$_2$O measurements, respectively; A_c and A_w are their respective remaining power values after the

215 source lights pass through the measured air sample; S_w is cross-sensitivity of the detector to H$_2$O, while detecting CO$_2$, at the wavelength for CO$_2$ measurements (hereafter referred to as sensitivity-to-H$_2$O); Z_c is the CO$_2$ zero adjustment (i.e., CO$_2$ zero coefficient); and G_c is the CO$_2$ gain adjustment (i.e., commonly known as the CO$_2$ span coefficient). For an individual analyzer, the parameters a_{ci}, Z_c, G_c, and S_w in Model (5) are statistically estimated in the production calibration against a series of standard CO$_2$ gases at different concentration levels over the ranges of ρ_{H2O} and P (hereafter referred to as

220 calibration). Since the estimated parameters are specific for the analyzer, Model (5) with these estimated parameters becomes an analyzer-specific CO$_2$ working equation. The working equation is used internally by the infrared analyzer to compute ρ_{CO_2} from field measurements of A_c, A_{cs}, A_w, A_{ws}, and P.

The analyzer-specific working equation is deemed to be accurate immediately after the calibration through estimations of a_{ci}, Z_c, G_c, and S_w in production while Z_c and G_c can be re-estimated in the field (LI−COR Biosciences, 2021b). However,

225 as used internally by an optical instrument under changing environments vastly different from its manufacturing conditions,

the working equation may not be fully adaptable to the changes, which might be reflected through CO_2 zero and/or gain drifts of the deployed infrared analyzers. In the working equation for ρ_{CO_2} from Model (5), the parameter Z_c is related to CO_2 zero drift; G_c, to CO_2 gain drift; and S_w, to sensitivity-to-H_2O. Therefore, the analyses of Z_c and G_c, along with S_w, are an approach to understand the causes of CO_2 zero drift, CO_2 gain drift, and sensitivity-to-H_2O. Such understanding is necessary to formulate $\Delta\rho^z_{CO_2}$, $\Delta\rho^g_{CO_2}$, and $\Delta\rho^s_{CO_2}$ in Model (3).

4.1 Z_c and $\Delta\rho^z_{CO_2}$ (CO_2 zero drift uncertainty)

In production, an infrared analyzer was calibrated for zero air/gas to report zero ρ_{CO_2} plus an unaviodable random error. However, when using of the analyzer in measurement environments that are different from calibration conditions, the analyzer often reports this zero ρ_{CO_2} value, while exposed to zero air, gradually away from zero and possibly beyond $\pm\Delta\rho^p_{CO_2}$, which is known as CO_2 zero drift. This drift is primarily affected by a collection of the three factors: i) the temperature surrounding the analyzer away from the calibration temperature, ii) traceable CO_2 and H_2O accumulations, during use, inside the analyzer light housing due to an inevitable, although extremely little, leaking exchange of housing air with ambient air (hereafter referred to as housing CO_2-H_2O accumulation), and iii) aging of analyzer components (Richardson et al., 2012)

Firstly, the dependency of analyzer CO_2 zero drift on ambient air temperature arises due to a thermal expansion/contraction of analyzer components that slightly changes the analyzer geometry (Fratini et al., 2014). This change in geometry can deviate the light path length for measurement a little away from the length under manufacturer calibration, contributing to the drift. Additionally, inside an analyzer, the performance of the light source and absorption detector for measurement, as well as the electronic components for measurement control, can vary slightly with temperature. In production, an analyzer is calibrated to compensate for the ensemble of such dependencies as assessed in a calibration chamber. The compensation algorithms are implemented in the analyzer operating system, which is kept as proprietary by the analyzer manufacturer. However, the response of an analyzer to a temperature varies as conditions change over time (Fratini et al., 2014). Therefore, manufacturers typically specify an expected range of typical or maximal drift per ºC (see Table 1). Secondly, the housing CO_2-H_2O accumulation is caused by unavoidable little leaks in the light housing of an infrared analyzer. The housing is technically sealed to keep housing air close to zero air by implementing scrubber chemicals into the housing to absorb any CO_2 and H_2O that may sneak into the housing through an exchange with any ambient air (LI−COR Biosciences, 2021b). Over time, the scrubber chemicals may be saturated by CO_2 and/or H_2O or lose their active absorbing effectiveness, which can result in housing CO_2-H_2O accumulations. Thirdly, as optical components, the light source may gradually become dim, and the absorption detector may gradually become less sensitive. The accumulation and aging develop less obviously and slowly in the relative long term (e.g., months or longer), whereas the dependencies of drift on ambient air temperature occur obviously and quickly as soon as an analyzer is deployed in the field (Richardson et al., 2012). Apparently, the drift with ambient air temperature is a major concern if an analyzer is maintained as scheduled (Campbell Scientific Inc., 2021b).

Due to the CO_2 zero drift, the working equation needs to be adjusted through its parameter re-estimation to adapt the ambient air temperature near which the system is running, housing $CO_2–H_2O$ accumulation, and analyzer component aging. This adjustment technique the working equation is the zero procedure, which brings the ρ_{CO_2} and ρ_{H_2O} in zero air/gas measurement back to zero as closely as possible. In this section, our discussion focus will focus on CO_2, and the same application to H_2O will be described in following sections. In the field, the zero procedure should be feasibly operational using one air/gas benchmark to re-estimate one parameter in the working equation. This parameter must be adjustable to output zero ρ_{CO_2} from the zero air/gas benchmark. By setting the left side of Eq. (5) to zero and re-arranging it, it is clear that Z_c is such a parameter that can be adjusted to result in a zero ρ_{CO_2} value for zero air/gas,

$$Z_c = \left[\frac{A_{c0}}{A_{cs}} + S_w \left(1 - \frac{A_{w0}}{A_{ws}} \right) \right]^{-1}, \tag{6}$$

where A_{c0} and A_{w0} are the counterparts of A_c and A_w for zero air/gas, respectively. For an analyzer, the zero procedure for CO_2 is thus to re-estimate Z_c in balance of Eq. (6).

If Z_c could continually balance Eq. (6) after the zero procedure, the CO_2 zero drift would not be significant; however, this is not the case. Similar to its performance after calibration, an analyzer may still drift after the zero procedures due to changing ambient air temperature, $CO_2–H_2O$ accumulation, and/or analyzer component aging. Nevertheless, the value of Z_c, is unpredictable because of the constant changes of ambient conditions surrounding the infrared analyzer, the housing $CO_2–H_2O$ accumulation, and analyzer component aging. Assuming on-schedule maintenance, i.e., the scrubber chemicals inside the analyzer light housing is replaced following the manufacture's guidelines, the housing $CO_2–H_2O$ accumulation should not be a concern. While the ambient temperature surrounding the infrared analyzer is not controlled, the CO_2 zero drift is therefore mainly influenced by T_a and can be ± 0.55 mgCO_2 m^{-3} at the most within the operational ranges in T_a and P for OPEC systems (Table 1).

Given that an analyzer performs best almost without zero drift at the ambient air temperature for the calibration/zeroing procedure (T_c), and that it possibly drifts while T_a gradually changes away from T_c, then the further away T_a is from T_c, the more it possibly drifts in the CO_2 zero. Over the operational range in P of EC150 infrared ananlyzers used for OPEC systems, this drift is more proportional to the difference between T_a and T_c but is still within the specifications (Campbell Scientific Inc., 2021b). Accordingly, CO_2 zero drift uncertainty at T_a can be formulated as

$$\Delta\rho_{CO_2}^z = \frac{d_{cz}}{T_{rh} - T_{rl}} \times \begin{cases} T_a - T_c & T_c < T_a < T_{rh} \\ T_c - T_a & T_c > T_a > T_{rl} \end{cases}, \tag{7}$$

where, over the operational range in T_a of EC150 infrared analyzers used for OPEC systems, T_{rh} is the highest-end value (50 °C) and T_{rl} is the lowest-end value (–30 °C, Table 1). $\Delta\rho_{CO_2}^z$ from this equation has the maximum range, as specified in Table 1, equal to d_{cz} in magnitude as if T_a and T_c were separately at the two ends of operational range in T_a of OPEC systems.

4.2 G_c and $\Delta\rho_{CO_2}^g$ (CO₂ gain drift uncertainty)

An infrared analyzer was also calibrated against a series of standard CO₂ gases. The calibration sets the working equation from Model (5) to closely follow the gain trend of change in ρ_{CO_2}. As was determined with the zero drift, the analyzer, with changes in internal CO₂−H₂O accumulation and ambient conditions during its deployment, could report CO₂ gradually
290 drifting away from the real gain trend of the change in ρ_{CO_2}, which is specifically termed CO₂ gain drift. This drift is affected by almost the same factors as the CO₂ zero drift (Richardson et al., 2012; Fratini et al., 2014; LI−COR Biosciences, 2021b).

Due to the gain drift, the infrared analyzer needs to be further adjusted, after the zero procedure, to tune its working equation back to the real gain trend in ρ_{CO_2} of measured air as close as possible. This is done with the CO₂ span procedure.
295 This procedure can be performed through use of either one or two span gases (LI−COR Biosciences, 2021b). If two are used, one span gas is slightly below the ambient CO₂ density and the other is at a much higher density to fully cover the CO₂ density range by the working equation. However, commonly, like the zero procedure, this procedure is simplified by the use of one CO₂ span gas, as a benchmark, with a known CO₂ density ($\tilde{\rho}_{CO_2}$) around the typical CO₂ density values in the measurement environment. Moreover, because only one CO₂ value from CO₂ span gas is used, only one parameter in the
300 working equation is available for adjustment. Weighing the gain of the working equation more than any other parameter, this parameter is the CO₂ span coefficient (G_c) (see Model (5)). The CO₂ span gas is used to re-estimate G_c to satisfy the following equation (for details, see LI−COR Biosciences, 2021b)

$$\left| \tilde{\rho}_{CO_2} - \rho_{CO_2}(G_c) \right| \leq \min \left| \tilde{\rho}_{CO_2} - \rho_{CO_2} \right|. \tag{8}$$

Similar to the zero drift, the CO₂ gain drift continues after the CO₂ span procedure. Based on a similar consideration
305 for the specifications of CO₂ zero drift, the CO₂ gain drift is specified by the maximum CO₂ gain drift percentage (δ_{CO2_g} = 0.1%) associated with ρ_{CO_2} as ±0.10%×(true ρ_{CO_2}) (Table 1). This specification is the maximum range of CO₂ measurement uncertainty due to the CO₂ gain drift within the operational ranges in T_a and P of OPEC systems.

Given that an analyzer performs best, almost without gain drift, at the ambient air temperature for calibration/span procedure (also denoted by T_c, because zero and span procedures should be performed under similar ambient air temperature
310 conditions) but also drifts while T_a gradually changes away from T_c, then the further away T_a is from T_c, the greater potential the drift has. Accordingly, the same approach to the formulation of CO₂ zero drift uncertainty can be applied to the formulation of approximate equation for CO₂ gain drift uncertainty at T_a as

$$\Delta\rho_{CO_2}^g \equiv \pm\frac{\delta_{CO_2\_g}\rho_{CO_2T}}{T_{rh} - T_{rl}} \times \begin{cases} T_a - T_c & T_c < T_a < T_{rh} \\ T_c - T_a & T_c > T_a > T_{rl} \end{cases}, \tag{9}$$

where ρ_{CO2T} is true CO₂ density unknown in measurement. Given that the measured value of CO₂ density is represented by
315 ρ_{CO_2}, by referencing Eq. (1), ρ_{CO2T} can be expressed as

11

$$\rho_{CO_2T} = \rho_{CO_2} - (\Delta\rho_{CO_2}^z + \Delta\rho_{CO_2}^g + \Delta\rho_{CO_2}^s + \Delta\rho_{CO_2}^p). \tag{10}$$

The terms inside the parentheses in this equation are the measurement uncetrainties for ρ_{CO2T} that are smaller in magnitude, by at least two orders, than ρ_{CO2T}, whose magnitude in atmospheric background under the normal temperature and pressure as used by Wright et al. (2003) is 760 mgCO$_2$ m^{-3} (Global Monitoring Laboratory, 2021). Therefore, ρ_{CO_2} in Eq. (10) is the best

320   alternative, with the most likelihood, to ρ_{CO2T} for the application of Eq. (9). As such, ρ_{CO2T} in Eq. (9) can be reasonably approximated by ρ_{CO2} for equation applications. Using this approximation, Eq. (9) becomes

$$\Delta\rho_{CO_2}^g = \pm\frac{\delta_{CO_2\_g}\rho_{CO_2}}{T_{rh} - T_{rl}} \times \begin{cases} T_a - T_c & T_c < T_a < T_{rh} \\ T_c - T_a & T_c > T_a > T_{rl} \end{cases}. \tag{11}$$

With ρ_{CO2} being measured, this equation is applicable in estimating the CO$_2$ gain drift uncertainty. The gain drift uncertainty ($\Delta\rho_{CO_2}^g$) from this equation has the maximum range of $\pm\delta_{CO2\_g}\,\rho_{CO2}$, as if T_a and T_c were separately at the two ends of

325   operational range in T_a of OPEC systems. With the most likelihood, this maximum range is the closest to $\pm\delta_{CO2\_g}\times$(true ρ_{CO2}) as specified in Table 1.

4.3 S_w and $\Delta\rho_{CO_2}^s$ (sensitivity-to-H$_2$O uncertainty)

The infrared wavelength of 4.3μm for CO$_2$ measurements is minorly absorbed by H$_2$O (LI−COR Biosciences, 2021b; Campbell Scientific Inc., 2021b). This minor absorption slightly interferes with the absorption by CO$_2$ in the wavelength

330   (McDermitt et al., 1993). The power of the same measurement light through several gas samples with the same CO$_2$ density, but different backgrounds of H$_2$O densities, is detected with different values of A_c for the working equation from Model (5). Without parameter S_w and its joined term in the working equation, different A_c values must result in significantly different ρ_{CO2} values, although they are actually the same. To report the same ρ_{CO2} for air flows with the same CO$_2$ density under different H$_2$O backgrounds, the different values of A_c to report similar ρ_{CO2} are accounted for by S_w associated with A_w and

335   A_{ws} in the working equation from Model (5). Similar to Z_c and G_c in the equation, S_w is not perfectly accurate and can have uncertainty in the determination of ρ_{CO2}. This uncertainty for EC150 infrared analyzers is specified by sensitivity-to-H$_2$O (s_{H2O}) as $\pm2.69\times10^{-7}$ mgCO$_2$ m^{-3} (gH$_2$O m^{-3})$^{-1}$ (Table 1). As indicated by its unit, this uncertainty is linearly related to ρ_{H2O}. Assuming the analyzer for CO$_2$ works best, without this uncertainty, in dry air, $\Delta\rho_{CO_2}^s$ could be formulated as

$$\Delta\rho_{CO_2}^s \equiv s_{H_2O}\rho_{H_2O} \quad 0 \le \rho_{H_2O} \le 44\,\text{gH}_2\text{O m}^{-3}, \tag{12}$$

340   where 44 gH$_2$O m^{-3}, as addressed in section 2, is a threshold for H$_2$O density measurements. Accordingly, $\Delta\rho_{CO_2}^s$ can be in a range of

$$\Delta\rho_{CO_2}^s \le 44\left|s_{H_2O}\right|. \tag{13}$$

4.4 $\Delta\rho_{CO_2}$ (CO₂ measurement accuracy)

Substituting Eqs. (4), (7), (11), and (13) into Model (3), $\Delta\rho_{CO_2}$ for an individual CO₂ measurement can be expressed as

$$\Delta\rho_{CO_2} = \pm\left[1.96\sigma_{CO_2} + 44\left|s_{H_2O}\right| + \frac{\left|d_{cz}\right| + \delta_{CO_2\_g}\rho_{CO_2}}{T_{rh} - T_{rl}} \times \begin{cases} T_a - T_c & T_c < T_a < T_{rh} \\ T_c - T_a & T_c > T_a > T_{rl} \end{cases}\right]. \qquad (14)$$

This is the CO₂ accuracy equation for EC150 infrared analyzers within OPEC systems. It expresses the accuracy of a field CO₂ measurement from the OPEC systems in terms of its specifications σ_{CO_2}, s_{H_2O}, d_{cz}, $\delta_{CO_2\_g}$, and the OPEC system operational range in T_a as indicated by T_{rh} and T_{rl}; measured variables ρ_{CO_2} and T_a; and a known variable T_c. Given the specifications and the known variable, this equation can be used to evaluate the CO₂ accuracy as a range in relation to T_a and ρ_{CO_2}.

4.5 Evaluation of $\Delta\rho_{CO_2}$

Given the analyzer specifications, the accuracy of field CO₂ measurements from an infrared analyzer after calibration, zero, and/or span at T_c can be evaluated using the CO₂ accuracy equation (14) over a domain of T_a and ρ_{CO_2}. To visualize the relationship of accuracy with T_a and ρ_{CO_2}, the accuracy is presented better as the ordinate along the abscissa of T_a for ρ_{CO_2} at different levels and must be evaluated within possible maximum ranges of T_a and ρ_{CO_2} in ecosystems. In evaluation, the T_a is limited to the –30 to 50 °C range within which EC150 infrared analyzers used for OPEC systems operate, T_c can be assumed to be 20 ºC (i.e., standard air temperature as used by Wright et al. (2003)), and ρ_{CO_2} can be ranged acoording to its variation in ecosystems.

4.5.1 ρ_{CO_2} range

Upper measurement limit of CO₂ density by the infrared analyzers can reach up to 1,553 mgCO₂ m⁻³. In the atmosphere, its CO₂ background mixing ratio currently is 415 µmolCO₂ mol⁻¹ (Global Monitoring Laboratory, 2021). Under the normal temperature and pressure conditions (Wright et al., 2003), this background mixing ratio is equivalent to 760 mgCO₂ m⁻³ in dry air. CO₂ density in ecosystems commonly ranges from 650 to 1,500 mgCO₂ m⁻³ (LI−COR Biosciences, 2021b), depending on biological processes (Wang et al., 2016), aerodynamic regimes (Yang et al., 2007), and thermodynamic states (Ohkubo et al., 2008). In this study, this range is extended from 600 to 1,600 mgCO₂ m⁻³ as a common range within which $\Delta\rho_{CO_2}$ is evaluated. Because of the dependence of $\Delta\rho_{CO_2}$ on ρ_{CO_2} (Eq. 14), to show the accuracy at different CO₂ levels, the range is further divided into five grades of 600, 760 (atmospheric background), 1000, 1300, and 1600 mgCO₂ m⁻³ for evaluation presentations as in Fig. 2.

According to a brief review by Zhou et al. (2021) on the plant physiological threshold in air temperature for growth and development and the soil temperature dynamic related to CO₂ from microorganism respiration and/or wildlife activities in terrestrial ecosystems, ρ_{CO_2} at any grade of 1,000, 1300, or 1600 mgCO₂ m⁻³ should start, at 5 ºC, to converge

asymptotically to the atmospheric CO_2 background (760 mgCO$_2$ m^{-3} at –30 ºC, Fig. 2). Without the asymptotical function for the convergence curve, conservatively assuming the convergence has a simple linear trend with T_a from 5 to –30 ºC, $\Delta\rho_{CO_2}$ is evaluated up to the magnitude of ρ_{CO_2} along the trend (Fig. 2).

375 **4.5.2 $\Delta\rho_{CO_2}$ range**

At $T_a = T_c$, the CO_2 accuracy is best at its narrowest range as the sum of precision and and sensitivity-to-H$_2$O uncertainties (±0.39 mgCO$_2$ m^{-3}). However, away from T_c, its range near-linearly becomes wider. The $\Delta\rho_{CO_2}$ range can be summarized as ±0.40 − ±1.21 mgCO$_2$ m^{-3} over the domain of T_a and ρ_{CO_2} (Fig. 2a and CO_2 columns in Table 2). The maximum CO_2 relative accuracy at the different levels of ρ_{CO_2} is in a range of ±0.07% at 1,600 mgCO$_2$ m^{-3} to 0.19% at 600 mgCO$_2$ m^{-3} (from data 380 for Fig. 2b).

14
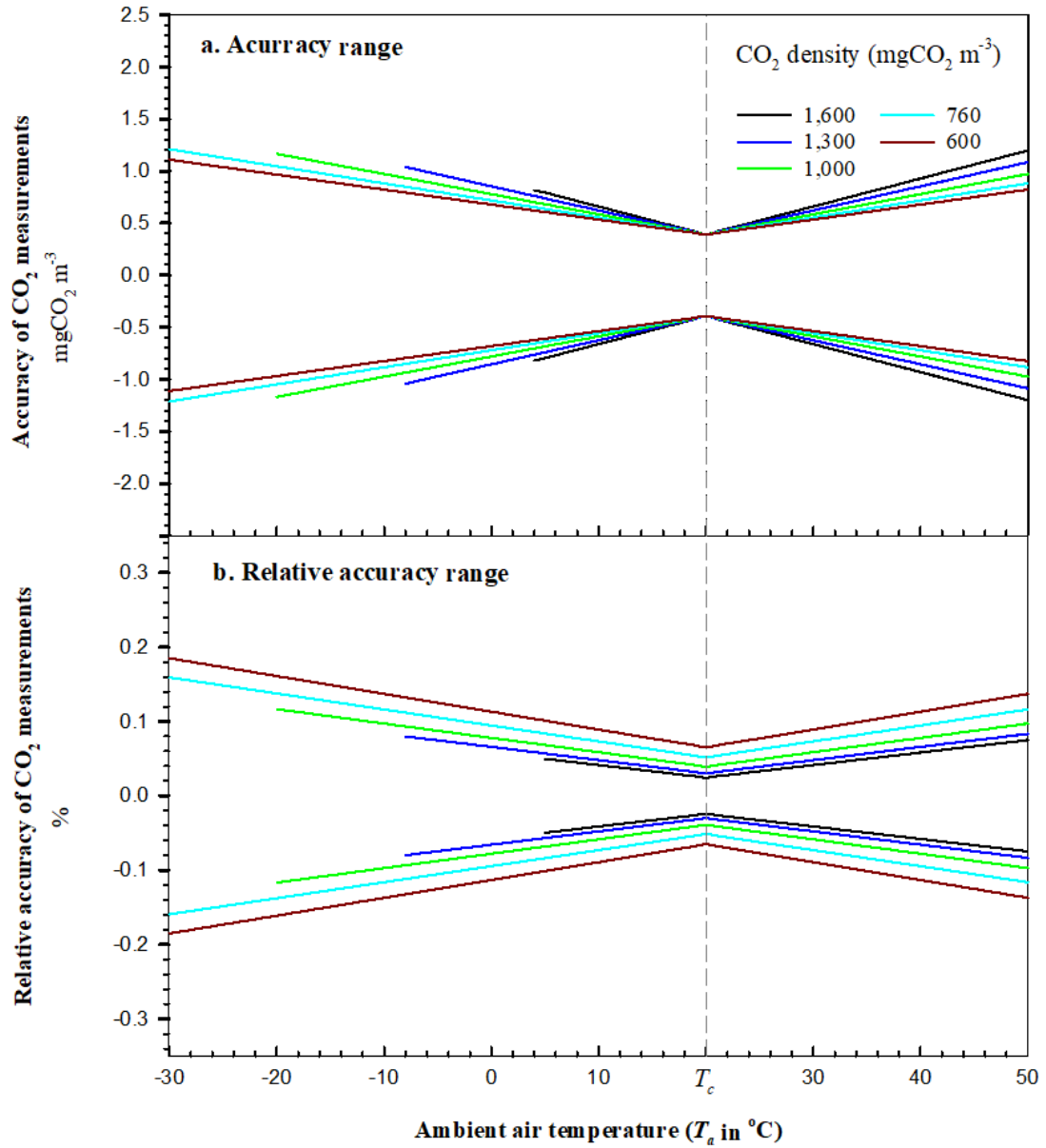
Figure 2. Accuracy of field CO_2 measurements from open-path eddy-covariance flux systems by EC150 infrared CO_2–H_2O analyzers over their operational range in T_a at atmospheric pressure of 101.325 kPa. The vertical dashed line represents ambient temperature T_c at which an analyzer was calibrated, zeroed, and/or spanned. Above 5 °C, accuracy is evaluated up to the possible maximum CO_2 density in ecosystems (black curve). Assume that this maximum CO_2 density starts linearly decreasing at 5 °C to the atmospheric CO_2 background value 760 $mgCO_2$ m^{-3} at –30 °C. Accordingly, below 5 °C, the accuracy for CO_2 density at a level above the background value (green, blue, or black curve) is evaluated up to this decreasing trend of CO_2 densities. Relative accuracy of CO_2 measurements is the ratio of CO_2 accuracy to CO_2 density.

15

Table 2. Accuracies of field CO_2 and H_2O measurements from open-path eddy-covariance systems by EC150 infrared $CO_2–H_2O$ analyzers on the major values of background ambient air temperature, CO_2, and H_2O in ecosystems. (Atmospheric pressure: 101.325 kPa. Calibration ambient air temperature: 20 ºC.)

Ambient air temperature	CO2				H2O			
	760 $mgCO_2$ m^{-3} [a/]		1,600 $mgCO_2$ m^{-3} [b/]		60% Relative humidity		Saturated	
	Accuracy ±	Relative accuracy ±	Accuracy ±	Relative accuracy ±	Accuracy ±	Relative accuracy ±	Accuracy ±	Relative accuracy ±
°C	$mgCO_2$ m^{-3}	%	$mgCO_2$ m^{-3}	%	gH_2O m^{-3}	%	gH_2O m^{-3}	%
−30	1.211	0.16			0.066	32.14	0.066	19.36
−25	1.129	0.15			0.063	19.01	0.064	11.47
−20	1.047	0.14			0.061	11.46	0.062	6.94
−15	0.965	0.13	N/A[c/]		0.059	7.04	0.060	4.28
−10	0.883	0.12			0.057	4.40	0.058	2.68
−5	0.801	0.11			0.055	2.79	0.056	1.71
0	0.720	0.09			0.052	1.80	0.054	1.11
5	0.638	0.08	0.795	0.05	0.050	1.22	0.052	0.76
10	0.556	0.07	0.661	0.04	0.047	0.84	0.049	0.52
15	0.474	0.06	0.526	0.03	0.044	0.57	0.045	0.35
20	0.392	0.05	0.392	0.02	0.040	0.39	0.040	0.23
25	0.474	0.06	0.526	0.03	0.045	0.33	0.047	0.20
30	0.556	0.07	0.661	0.04	0.052	0.29	0.057	0.19
35	0.638	0.08	0.795	0.05	0.061	0.26	0.070	0.18
37	0.670	0.09	0.849	0.05	0.066	0.25	0.077	0.17
40	0.720	0.09	0.930	0.06	0.073	0.24		
45	0.801	0.11	1.064	0.07	0.090	0.23	N/A[d/]	
48	0.851	0.11	1.145	0.07	0.099	0.23		
50	0.883	0.12	1.198	0.07	N/A[e/]			

[a] 760 $mgCO_2$ m^{-3} is the atmospheric background CO_2 density.

[b] 1,600 $mgCO_2$ m^{-3} is assumed to be the maximum CO_2 density in ecosystems.

[c] CO_2 density in ecosystems is assumed to be lower than 1,600 $mgCO_2$ m^{-3} when ambient air temperatures is below 5 °C.

[d] H_2O density in saturated air above 37 °C is out of the measurement range of EC150 infrared $CO_2–H_2O$ analyzers (0 − 44 gH_2O m^{-3}).

[e] H_2O density in air of 60% relative humidity above 48 °C is out of the measurement range of EC150 infrared $CO_2–H_2O$ analyzers (0 − 44 gH_2O m^{-3}).

5 Accuracy of H₂O density measurements

Model (2) defines the accuracy of field H_2O measurements from OPEC systems by infrared analyzers ($\Delta\rho_{H_2O}$) as

$$\Delta\rho_{H_2O} \equiv \pm\left(\left|\Delta\rho_{H_2O}^z\right| + \left|\Delta\rho_{H_2O}^g\right| + \left|\Delta\rho_{H_2O}^s\right| + \left|\Delta\rho_{H_2O}^p\right|\right), \tag{15}$$

where $\Delta\rho_{H_2O}^z$ is H₂O zero drift uncertainty, $\Delta\rho_{H_2O}^g$ is H₂O gain drift uncertainty, $\Delta\rho_{H_2O}^s$ is cross-sensitivity-to-CO₂ uncertainty,

and $\Delta\rho_{H_2O}^p$ is H₂O precision uncertainty. Using the same approach as for $\Delta\rho_{CO_2}^p$, $\Delta\rho_{H_2O}^p$ is formulated as

$$\Delta\rho_{H_2O}^P = \pm 1.96 \times \sigma_{H_2O}, \tag{16}$$

where σ_{H2O}, as defined in Table 1, is the precision of EC150 analyzers for H₂O measurements. The other uncertainty terms in Model (15) can be understood and formulated using the similar approach for their counterparts in Model (3).

5.1 $\Delta\rho_{H_2O}^z$ (H₂O zero drift uncertainty) and $\Delta\rho_{H_2O}^g$ (H₂O gain drift uncertainty)

The model of the analyzer working equation for ρ_{H2O} is similar to Model (5) for ρ_{CO2} in formulation, given also by the derivations in the Theory and operation section in LI−COR Biosciences (2001, 2021a, 2021b)

$$\rho_{H_2O} = P\sum_{i=1}^{3} a_{wi}\left\{1 - \left[\frac{A_w}{A_{ws}} + S_c\left(1 - \frac{A_c}{A_{cs}}\right)\right]Z_w\right\}^i \left\{\frac{G_w}{P}\right\}^i, \tag{17}$$

where a_{wi} (i = 1, 2, or 3) is a coefficient of the three-order polynomial in the terms inside curly brackets; S_c is the cross-sensitivity of a detector to CO₂, while detecting H₂O, at the wavelength for H₂O measurements (hereafter referred to as sensitivity-to-CO₂); Z_w is the H₂O zero adjustment (i.e., H₂O zero coefficient); G_w is the H₂O gain adjustment (i.e., commonly referred as to H₂O span coefficient); and A_w, A_{ws}, A_c, and A_{cs} represent the same as in Model (5). The parameters of a_{wi}, Z_w G_w, and S_c in Model (17) are statistically estimated to establish an H₂O working equation in production calibration against a series of air standards with different H₂O contents under ranges of ρ_{CO2} and P (i.e., calibration). The H₂O working equation (i.e., Model 17 with estimated parameters) is used inside the analyzer to compute ρ_{H2O} as the closest proxy for true ρ_{H2O} from field measurements of A_w, A_{ws}, A_c, A_{cs}, and P.

Because of the similarities in model principles and parameter implications between Models (5) and (17), following the same analyses and rationales as for $\Delta\rho_{CO_2}^z$ and $\Delta\rho_{CO_2}^g$, $\Delta\rho_{H_2O}^z$ is formulated as

$$\Delta\rho_{H_2O}^z = \frac{d_{wz}}{T_{rh} - T_{rl}} \times \begin{cases} T_a - T_c & T_c < T_a < T_{rh} \\ T_c - T_a & T_c > T_a > T_{rl} \end{cases}, \tag{18}$$

and $\Delta\rho_{H_2O}^g$ is formulated as

$$\Delta\rho_{H_2O}^g = \pm\frac{\delta_{H_2O\_g}\rho_{H_2O}}{T_{rh} - T_{rl}} \times \begin{cases} T_a - T_c & T_c < T_a < T_{rh} \\ T_c - T_a & T_c > T_a > T_{rl} \end{cases}. \tag{19}$$

5.2 $\Delta\rho_{H_2O}^s$ (sensitivity-to-CO₂ uncertainty)

The infrared light at wavelength of 2.7 μm for H_2O measurement is traceably absorbed by CO_2 (see Fig. 4.7 in Wallace and Hobbs, 2006). This absorption interferes slightly with the H_2O absorption at this wavelength (McDermitt et al., 1993). As such, the power of identical measurement lights through several air standards with the same H_2O density but different backgrounds of CO_2 amounts would result in different values of A_w into the H_2O working equation from Model (17). In this equation, without parameter S_c and its joined term, different A_w values will result in significantly different ρ_{H_2O} values, although ρ_{H_2O} is essentially the same. To report the same ρ_{H_2O} for air flows with the same H_2O amount under different CO_2 backgrounds, different values of A_w to report the same ρ_{H_2O} are accounted for by S_c associated with A_c and A_{cs} in the H_2O working equation (see Model 17). However, S_c is not perfectly accurate, either, having uncertainty in the determination of ρ_{H_2O}. This uncertainty in the EC150 infrared analyzer is specified by the sensitivity-to-CO₂ (s_{CO_2}) value as the maximum range of $\pm 4.09 \times 10^{-5}$ gH_2O m^{-3} ($mgCO_2$ $m^{-3})^{-1}$ (Table 1). Assuming the infrared analyzers for H_2O have the lowest sensitivity-to-CO₂ uncertainty for air flow with an atmospheric background CO_2 amount (i.e., 760 $mgCO_2$ m^{-3}), $\Delta\rho_{H_2O}^s$ could be formulated as

$$\Delta\rho_{H_2O}^s = s_{CO_2}\left(\rho_{CO_2} - 760\right) \qquad \rho_{CO_2} \leq 1{,}553 \text{ mgCO}_2 \text{ m}^{-3}. \qquad (20)$$

Accordingly, $\Delta\rho_{H_2O}^s$ can be reasonably expressed as

$$\left|\Delta\rho_{H_2O}^s\right| \leq 793 s_{CO_2}. \qquad (21)$$

5.3 $\Delta\rho_{H_2O}$ (H₂O measurement accuracy)

Substituting Eqs. (16), (18), (19) and (21) into Model (15), $\Delta\rho_{H_2O}$ for an individual H_2O measurement from OPEC systems can be expressed as

$$\Delta\rho_{H_2O} = \pm\left[1.96\sigma_{H_2O} + 793\left|s_{CO_2}\right| + \frac{\left|d_{wz}\right| + \delta_{H_2O\_g}\rho_{H_2O}}{T_{rh} - T_{rl}} \times \begin{cases} T_a - T_c & T_c < T_a < T_{rh} \\ T_c - T_a & T_c > T_a > T_{rl} \end{cases} \right]. \qquad (22)$$

This equation is the H_2O accuracy equation for the OPEC systems with infrared analyzers. It expresses the accuracy of H_2O measurements from the OPEC systems in terms of the specifications σ_{H_2O}, s_{CO_2}, d_{wz}, $\delta_{H_2O\_g}$, T_{rh}, and T_{rl}; measured variables ρ_{H_2O} and T_a; and a known variable T_c. Using this equation and the specification values as in Table 1 for EC150 infrared analyzers, the accuracy of field H_2O measurements can be evaluated as a range for OPEC systems with such anlyzers. For an OPEC system with another model of open-path infrared anlyzer, such as the LI−7500 series (LI−COR Biosciences, NE, USA) or IRGASON (Campbell Scientific Inc., UT, USA), its corresponding specification values are used.

5.4 Evaluation of $\Delta\rho_{H_2O}$

H_2O accuracy ($\Delta\rho_{H_2O}$) can be evaluated using the H_2O accuracy equation over a domain of T_a and ρ_{H_2O}. Similar to the CO_2 accuracy equation in Fig. 2, $\Delta\rho_{H_2O}$ is presented as the ordinate along the abscissa of T_a at different ρ_{H_2O} levels within the ranges of T_a and ρ_{H_2O} in ecosystems (Fig. 3). As with the evaluation of $\Delta\rho_{CO_2}$, T_a is limited from –30 to 50 °C and T_c can be assumed to be 20 ºC. The range of ρ_{H_2O} at T_a needs to be be determined using atmospheric physics (Buck, 1981).

5.4.1 ρ_{H_2O} range

The EC150 analyzers were calibrated for H_2O density from 0 to 44 gH_2O m^{-3} due to the reason addressed in Sect. 2. The highest limit of measurement range for H_2O density by other models of analyzers also should be near 44 gH_2O m^{-3}. However, due to the positive exponential dependence of air water vapor saturation on T_a (Wallace and Hobbs, 2006), ρ_{H_2O} has a range that is wider at higher T_a and narrower at lower T_a. Below 37 °C at 101.325 kPa, ρ_{H_2O} is lower than 44 gH_2O m^{-3}, and its range becomes narrower and narrower, reaching 0.34 gH_2O m^{-3} at –30 °C. To determine the H_2O accuracy over the same relative range of air moisture, even at different T_a, the water vapor saturation density is used to scale air moisture to 20, 40, 60, 80 and 100% (i.e., relative humidity, or RH). For each scaled RH value, ρ_{H_2O} can be calculated at different T_a and P (Appendix B) for use in the H_2O accuracy equation. In this way, over the range of T_a, H_2O accuracy can be shown as curves with equal RH (Fig. 3).

5.4.2 $\Delta\rho_{H_2O}$ range

In the same way as with CO_2 accuracy, the H_2O accuracy at $T_a = T_c$ is best at its narrowest as the sum of precision and sensitivity-to-CO_2 uncertainties (<0.040 gH_2O m^{-3} in magnitude). However, away from T_c, its non-linear range becomes wider, very gradually below this T_c value but more abruptly above, because, as T_a increases, ρ_{H_2O} at the same RH increases exponentially (Eqs. B1 and B2 in Appendix B) while $\Delta\rho_{H_2O}$ increases linearly with ρ_{H_2O} in the H_2O accuracy equation (22). This non-linear range can be summarized as the widest at 48 °C to be ±0.099 gH_2O m^{-3} for air with 60% RH (Fig. 3a and H_2O columns in Table 2). The number can be rounded up to ±0.10 gH_2O m^{-3} for the overall accuracy of field H_2O measurements from OPEC systems by the EC150 infrared analyzers.

Fig. 3b shows an interesting trend of H_2O relative accuracy with T_a. Given the RH range shown in Fig. 3b, the relative accuracy diverges with a T_a decrease and converges with a T_a increase. The H_2O relative accuracy varies from 0.17% for saturated air at 37 ºC to 96% for 20% RH air at –30 ºC (data for Fig. 3b) and, at this low T_a, can be much greater if RH goes further lower. The H_2O relative accuracy in magnitude is < 1% while ρ_{H_2O} > 5.00 gH_2O m^{-3}, < 5% while ρ_{H_2O} > 1.20 gH_2O m^{-3}, and >10% while ρ_{H_2O} < 0.60 gH_2O m^{-3}.
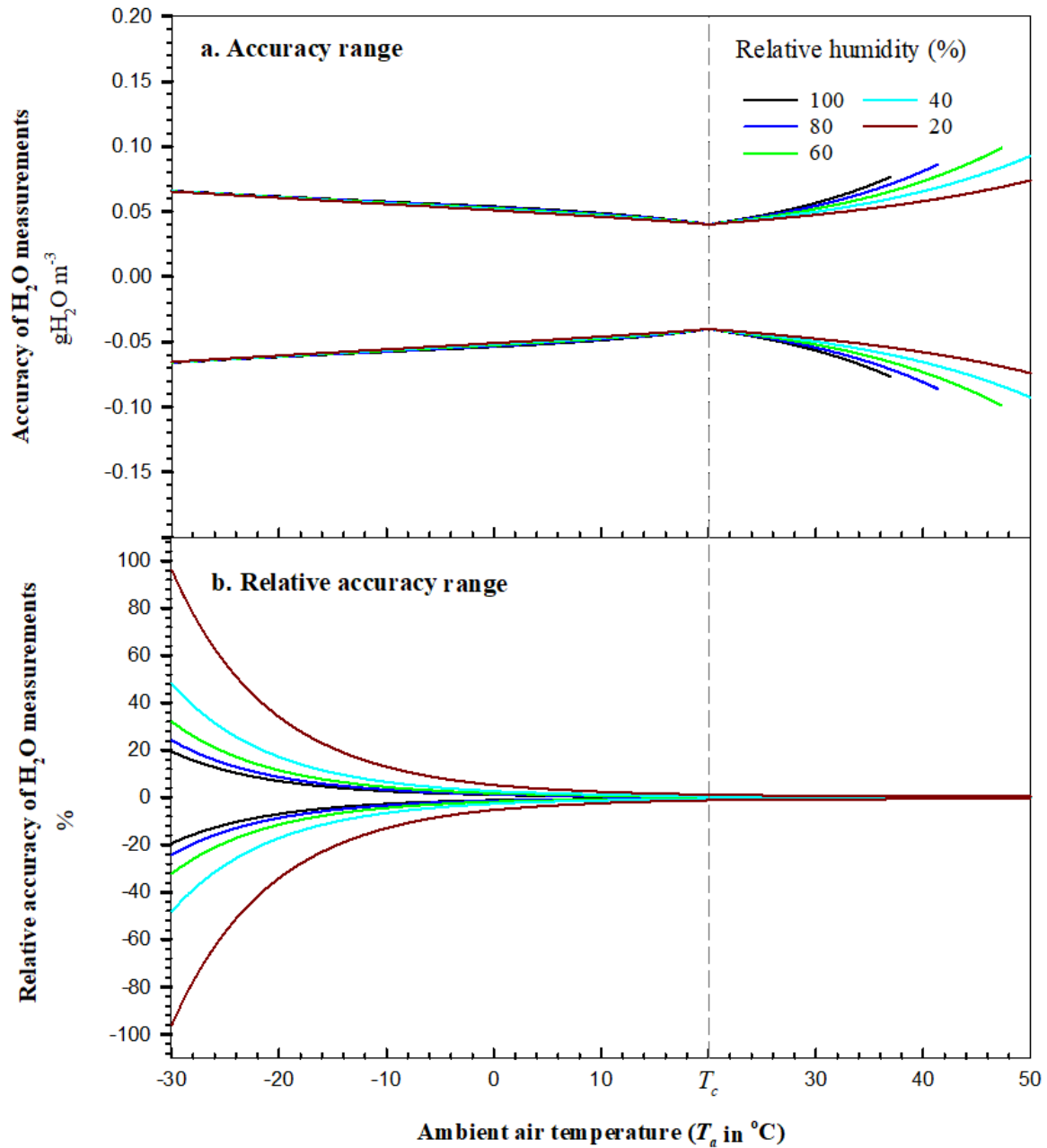
Figure 3. Accuracy of field H_2O measurements from open-path eddy-covariance systems by EC150 infrared CO_2–H_2O analyzers over their operational range in T_a under atmospheric pressure of 101.325 kPa. The vertical dashed line represents the ambient air temperature (T_c) at which an analyzer was calibrated, zeroed, and/or spanned. Relative accuracy of H_2O measurements is the ratio of H_2O accuracy to H_2O density.

480

6 Application

The primary objective of this study is to develop an assessment methodology to evaluate the overall accuracies of field CO_2 and H_2O measurements from the infrared analyzers in OPEC systems by compositing their individual measurement uncertainties as specified with four uncertainty descriptors: zero drift, gain drift, sensitivity-to-CO_2/H_2O, and precision variability (Table 1). The evaluated accuracy can be used to estimate the uncertainties of CO_2 and H_2O fluxes due to $\Delta\rho_{CO2}$ and $\Delta\rho_{H2O}$, assess CO_2 and H_2O data applications, and the formulated accuracy equations further provide rationales to assess and guide field maintenance on the infrared analyzers.

6.1 Conceptual models for estimating partial effects of $\Delta\rho_{CO2}$ and $\Delta\rho_{H2O}$ on uncertainty of hourly CO_2/H_2O flux

As discussed in Introduction, the uncertainty of each flux is contributed by numerous sub-uncertainties in the processes of measurements and computations, among which $\Delta\rho_{CO2}$ and $\Delta\rho_{H2O}$ are two fundamental uncertainties from infrared analyzers. Assume 3-D wind speeds are accurately measured, Appendix C demonstrates no effects of $\Delta\rho_{CO2}$ and $\Delta\rho_{H2O}$ on the uncertainty of the covariance of vertical wind speed (w) with ρ_{CO2}, ρ_{H2O}, or T_a until the covariance underwent through coordinate rotations (r), lag maximization (m), and low- and high-frequency (f) are finished. Equations (C8 and C9) give:

$$
\begin{aligned}
\overline{\left(w'\rho'_{CO_2}\right)}_{rmf} &= \overline{\left(w'\rho'_{CO_2 T}\right)}_{rmf} \\
\overline{\left(w'\rho'_{H_2O}\right)}_{rmf} &= \overline{\left(w'\rho'_{H_2OT}\right)}_{rmf} \\
\overline{\left(w'T'_a\right)}_{rmf} &= \overline{\left(w'T'_{aT}\right)}_{rmf}
\end{aligned}
\tag{23}
$$

where the overbar is an averaging operator, prime denotes the fluctuations of a variable away from its mean (e.g., $w'_i = w_i - \overline{w}$), subscript T indicates true value, and subscript rmf indicates the covariance was corrected through coordinate rotations (r), lag maximization (m), and low- and high-frequency (f) corrections. Further, through WPL correction, the three terms on the left side of Eq. (23) can be used to derive an analytical equation for CO_2 or H_2O flux from ρ_{CO2} and/or ρ_{H2O} with an error as ranged by its accuracy and T_a with an error whereas the three terms on the right side of this equation can be used to derive the equation from ρ_{CO2T}, ρ_{H2OT} and/or T_{aT}, all of which theoretically do not include errors. The comparison of both analytical equations can demonstrate the partial effects of $\Delta\rho_{CO2}$ and $\Delta\rho_{H2O}$ on uncertainty of hourly CO_2 or H_2O flux.

6.1.2 $\Delta\rho_{CO2}$ and $\Delta\rho_{H2O}$ on uncertainty of hourly CO_2 flux

Through WPL correction using the ρ_{H2O} and T_a related terms for ρ_{CO2} related term in Eq. (23), the measured CO_2 flux (F_{CO2}) is given by

$$
F_{CO_2} = \overline{\left(w'\rho'_{CO_2}\right)}_{rmf} + \left[\mu \frac{\overline{\rho}_{CO_2}}{\overline{\rho}_d} \overline{\left(w'\rho'_{H_2O}\right)}_{rmf} + \left(1 + \mu \frac{\overline{\rho}_{H_2O}}{\overline{\rho}_d}\right) \frac{\overline{\rho}_{CO_2}}{\overline{T}_a} \overline{\left(w'T'_a\right)}_{rmf} \right],
\tag{24}
$$

where μ is the ratio of dry air to water molecular weight and ρ_d is dry air density. Submitting Eqs. (1) and (23) leads to

$$F_{CO_2} = \overline{\left(w'\rho'_{CO_2T}\right)}_{rmf} +$$
$$\left[\mu\frac{\overline{\rho}_{CO_2T}+\Delta\overline{\rho}_{CO_2}}{\overline{\rho}_{dT}-\Delta\overline{\rho}_{H_2O}}\overline{\left(w'\rho'_{H_2OT}\right)}_{rmf} + \left(1+\mu\frac{\overline{\rho}_{H_2OT}+\Delta\overline{\rho}_{H_2O}}{\overline{\rho}_{dT}-\Delta\overline{\rho}_{H_2O}}\right)\frac{\overline{\rho}_{CO_2T}+\Delta\overline{\rho}_{CO_2}}{\overline{T}_{aT}+\Delta\overline{T}_a}\overline{\left(w'T'_{aT}\right)}_{rmf}\right] ,$$

(25)

where $\Delta\overline{T}_a$ is the uncertainty of $\overline{T}_a$. $\Delta\overline{T}_a$ is well defined as ±0.20 K in compliance with the WMO standard (WMO, 2018). According to Eq. (24), the nominate true CO_2 flux (F_{CO2T}) is given by

$$F_{CO_2T} = \overline{\left(w'\rho'_{CO_2T}\right)}_{rmf} + \left[\mu\frac{\overline{\rho}_{CO_2T}}{\overline{\rho}_{dT}}\overline{\left(w'\rho'_{H_2OT}\right)}_{rmf} + \left(1+\mu\frac{\overline{\rho}_{H_2OT}}{\overline{\rho}_{dT}}\right)\frac{\overline{\rho}_{CO_2T}}{\overline{T}_{aT}}\overline{\left(w'T'_{aT}\right)}_{rmf}\right] .$$

(26)

From Eqs (25) and (26), the uncertainty of CO_2 flux (ΔF_{CO2}) can be expressed as

$$\Delta F_{CO_2} = F_{CO_2} - F_{CO_2T}$$
$$= \mu\left(\frac{\overline{\rho}_{CO_2T}+\Delta\overline{\rho}_{CO_2}}{\overline{\rho}_{dT}-\Delta\overline{\rho}_{H_2O}} - \frac{\overline{\rho}_{CO_2T}}{\overline{\rho}_{dT}}\right)\overline{\left(w'\rho'_{H_2OT}\right)}_{rmf} +$$
$$\left[\left(1+\mu\frac{\overline{\rho}_{H_2OT}+\Delta\overline{\rho}_{H_2O}}{\overline{\rho}_{dT}-\Delta\overline{\rho}_{H_2O}}\right)\frac{\overline{\rho}_{CO_2T}+\Delta\overline{\rho}_{CO_2}}{\overline{T}_{aT}+\Delta\overline{T}_a} - \left(1+\mu\frac{\overline{\rho}_{H_2OT}}{\overline{\rho}_{dT}}\right)\frac{\overline{\rho}_{CO_2T}}{\overline{T}_{aT}}\right]\overline{\left(w'T'_{aT}\right)}_{rmf}$$

(27)

This derivation provides a conceptual model for the partial effects of $\Delta\rho_{CO2}$ and $\Delta\rho_{H2O}$ on the uncertainty of hourly CO_2 flux. This uncertainty is added by $\Delta\rho_{CO2}$ and $\Delta\rho_{H2O}$ through the density effect due to H_2O flux (1st term in Eq. 27) and temperature

flux (2nd term in Eq. 27).

6.1.2 $\Delta\rho_{H2O}$ on uncertainty of hourly H_2O flux

Using the same approach to Eq. (27), the uncertainty of H_2O flux (ΔF_{H2O}) can be expressed as

$$\Delta F_{CO_2} = \mu\left(\frac{\overline{\rho}_{H_2OT}+\Delta\overline{\rho}_{H_2O}}{\overline{\rho}_{dT}-\Delta\overline{\rho}_{H_2O}} - \frac{\overline{\rho}_{H_2OT}}{\overline{\rho}_{dT}}\right)\overline{\left(w'\rho'_{H_2OT}\right)}_{rmf} +$$
$$\left[\left(1+\mu\frac{\overline{\rho}_{H_2OT}+\Delta\overline{\rho}_{H_2O}}{\overline{\rho}_{dT}-\Delta\overline{\rho}_{H_2O}}\right)\frac{\overline{\rho}_{H_2OT}+\Delta\overline{\rho}_{H_2O}}{\overline{T}_{aT}+\Delta\overline{T}_a} - \left(1+\mu\frac{\overline{\rho}_{H_2OT}}{\overline{\rho}_{dT}}\right)\frac{\overline{\rho}_{H_2OT}}{\overline{T}_{aT}}\right]\overline{\left(w'T'_{aT}\right)}_{rmf}$$

(28)

This formulation provides a conceptual model for the partial effects of $\Delta\rho_{H2O}$ on the uncertainty of hourly H_2O flux. This

uncertainty is added only $\Delta\rho_{H2O}$ also through the density effect due to H_2O flux (1st term in Eq. 28) and temperature flux (2nd term in Eq. 28). Further analysis and more discussion about Eqs. (27) and (28) go beyond the scope of this study.

6.2 Application of H$_2$O accuracy in data use

The measured variables ρ_{H2O}, T_s and P can be used to compute T_a (Swiatek, 2018). If $T_a(\rho_{H_2O}, T_s, P)$ were an exact function from the theoretical principles, it would not have any error itself. However, in our applications, variables ρ_{H2O}, T_s, and P are measured from the OPEC systems experiencing seasonal climates. As addressed in this study, the measured values of these variables have measurement uncertainty in ρ_{H2O} ($\Delta\rho_{H2O}$, i.e., accuracy of field H$_2$O measurement); in T_s (ΔT_s, i.e., accuracy of field T_s measurement); and in P (ΔP, i.e., accuracy of field P measurement). The uncertainties from measurement propagate to the computed T_a as an uncertainty (ΔT_a, i.e., accuracy of $T_a(\rho_{H_2O}, T_s, P)$). This accuracy is a reference by any application of T_a. It should be specified through its relationship of ΔT_a to $\Delta\rho_{H2O}$, ΔT_s, and ΔP.

As field measurement uncertainties, $\Delta\rho_{H2O}$, ΔT_s, or ΔP are reasonably small increments in numerical analysis (Burden et al., 2016). As such, depending on all the small increments, ΔT_a is a total differential of $T_a(\rho_{H_2O}, T_s, P)$ with respect to ρ_{H2O}, T_s, and P, which are measured independently by three sensors, given by

$$\Delta T_a = \pm\left(\frac{\partial T_a}{\partial \rho_{H_2O}}\Delta\rho_{H_2O} + \frac{\partial T_a}{\partial T_s}\Delta T_s + \frac{\partial T_a}{\partial P}\Delta P\right). \tag{29}$$

In this equation, $\Delta\rho_{H2O}$ from the application of Eq. (22) is a necessary term to acquire ΔT_a, ΔT_s can be acquired from the specifications for 3-D sonic anemometers (Zhou et al., 2018), ΔP can be acquired from the specifications for the barometer used in the OPEC systems (Vaisala, 2020), and the three partial derivatives can be derived from the explicit function $T_a(\rho_{H_2O}, T_s, P)$. With $\Delta\rho_{H2O}$, ΔT_s, ΔP, and the three partial derivatives, ΔT_a can be ranged as a function of ρ_{H2O}, T_s, and P.

6.3 Application of accuracy equations in analyzer field maintenance

An infrared analyzer performs better if the field environment is near its manufacturing conditions (e.g., T_a at 20 °C), which is demonstrated in Figs. 2a and 3a for measurement accuracies associated with T_c. As indicated by the accuracies in both figures, the closer to T_c at 20 °C while T_a is, the better analyzers perform. However, the analyzers are mostly used in OPEC systems for long-term field campaigns through four-seasonal climates vastly different from those in the manufacturing processes. Over time, an analyzer gradually drifts in some ways and needs field maintenance although within its specifications.

The field maintenance cannot improve the sensitivity-to-CO$_2$/H$_2$O uncertainty and precision variability, but both are minor (their sum < 0.392 mgCO$_2$ m^{-3} for CO$_2$, Eqs. 4 and 13; < 0.045 gH$_2$O m^{-3} for H$_2$O, Eqs. 16 and 21) as compared to the zero or gain drift uncertainties. However, the zero and gain drift uncertainties are major in determination of field CO$_2$/H$_2$O measurement accuracy (Figs. 2 to 4 and Eqs. 14 and 22), but adjustable, through the zero and/or span procedures, to be minimized. Therefore, manufacturers of infrared analyzers have provided software and hardware tools for the procedures (Campbell Scientific Inc., 2021b) and scheduled the procedures using those tools (LI−COR Biosciences, 2021b). Fratini et

al. (2014) provided a technique implemented into the EddyPro program to correct the drift bias from a raw time series of CO_2 and H_2O data through post-processing. This study provides rationales how to assess, schedule, and perform the procedures (Figs. 2a, 3a, and 4).

6.3.1 CO_2 zero and span procedures

560 Figure 4a shows that the CO_2 zero drift uncertainty linearly increases with T_a away from T_c over the full T_a range within which OPEC systems operate; so, too, does CO_2 gain drift uncertainty increase for a given CO_2 concentration. As suggested by Zhou et al. (2021), both drifts should be adjusted near the T_a value around which the system runs. The zero and gain drifts should be adjusted, through zero and span procedures, at a T_a close to its daily mean around which the system runs. Based on the range of T_a daily cycle, the procedures are set at a moderate, instead of the highest or lowest, moment in T_a. Given the

565 daily cycle range is much narrower than 40 °C, an OPEC system could run at T_a within ±20 of T_c if the procedures are performed at a right moment of T_a. For our study case on atmospheric CO_2 background (left CO_2 column in Table 2), the procedures can narrow the widest possible range of ±1.21 $mgCO_2$ m^{-3} for field CO_2 measurement at least 40% to ±0.72 $mgCO_2$ m^{-3} (i.e., accuracy at 0 or 40 °C when T_c = 20 °C), which would be a significant improvement to ensure field CO_2 measurement accuracy through CO_2 zero and span procedures.

570 6.3.2 H_2O zero and span procedures

Figure 4b shows that the H_2O zero drift uncertainty increases as T_a moves away from T_c in the same trend as CO_2 zero drift uncertainty. Therefore, an H_2O zero procedure can be performed in the same technique as for CO_2 zero procedure. H_2O gain drift uncertainty has a different trend. It exponentially diverges, as T_a increases away from T_c, to ±5.0 × 10^{-2} gH_2O m^{-3} near 50 °C, and gradually converges by two orders smaller, as T_a decreases away from T_c, to ±6.38 × 10^{-4} gH_2O m^{-3} at −30 °C

575 (data for Fig. 4b). The exponential divergence results from the linear relationship of H_2O gain drift uncertainty (Eq. 19) with ρ_{H2O}, which exponentially increases (Eq. B1) with a T_a increase away from T_c for the same RH (Buck, 1981). The convergence results from the linear relationship offset by the exponential decrease in ρ_{H2O} with a T_a decrease for the same RH. This trend of H_2O gain drift uncertainty with T_a is a rationale to guide the H_2O span procedure, which adjusts the H_2O gain drift.

580 The H_2O span procedure needs standard moist air with known H_2O density from a dew point generator. The generator is not operational near or below freezing conditions (LI−COR Biosciences, 2004), which limits the span procedure to be performed only under non-freezing conditions. This condition, from 5 to 35 °C, may be considered for the generator to be conveniently operational in the field. Accordingly, the H_2O zero and span procedures should be discussed separately for a T_a above and below 5 °C.

24

6.3.2.1 T_a above 5 ºC

Looking at the right portion with T_a above 5 ºC in Fig. 4b, H_2O gain drift has a more obvious impact on measurement uncertainty in a higher T_a range (e.g., above T_c), within which the H_2O span procedure is most needed. In this range, the maximum accuracy range of ±0.10 gH_2O m^{-3} can be narrowed by 30% to ±0.07 (assessed from data for Fig 3a) if H_2O zero and span procedures can be sequentially performed as necessary in a T_a range from 5 to 35 ºC.

6.3.2.2 T_a below 5 ºC

Looking at the left portion with T_a below 5 ºC in Fig 4b, H_2O gain drift has a less obvious contribution to the measurement uncertainty in a lower T_a range (e.g., below 5 ºC), within which the H_2O span procedure may be unnecessary. An H_2O gain drift uncertainty at 5 ºC is 50% of the H_2O zero drift uncertainty (dotted curve in Fig. 5). This percentage decreases to 3% at –30 ºC. On average, this percentage over a range of –30 to 5 ºC is 18% (assessed from data for dotted curve in Fig. 5). Thus, for H_2O measurements over the lower T_a range, it can be concluded that H_2O zero drift is a major uncertainty source, and H_2O gain drift is a minor uncertainty source.
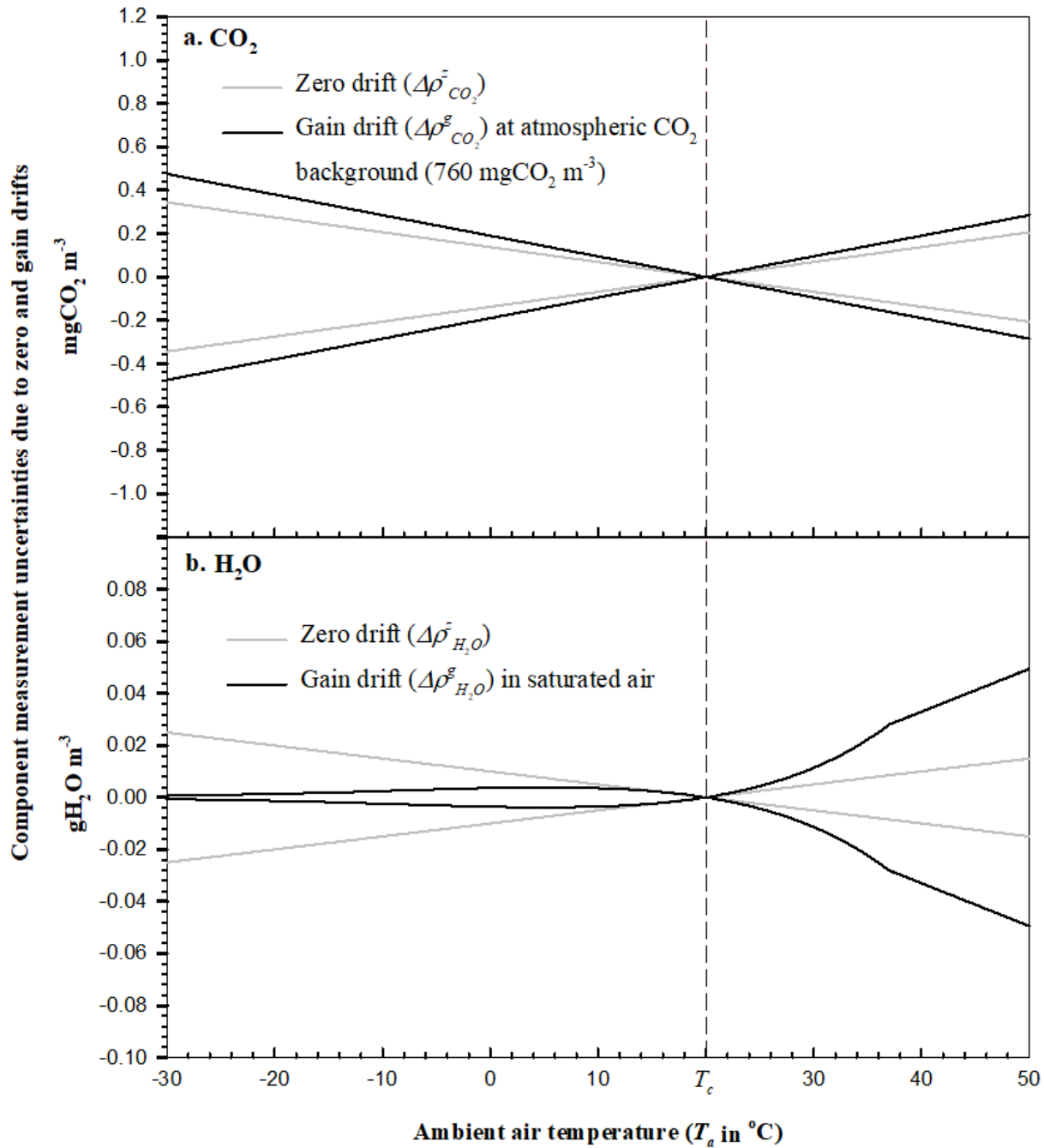
Figure 4. Component measurement uncertainties due to the zero and gain drifts of EC150 infrared CO_2–H_2O analyzers in open-path eddy-covariance flux systems over their operational range in T_a under an atmospheric pressure of 101.325 kPa. The vertical dashed line represents the ambient temperature (T_c) at which an analyzer was calibrated, zeroed, and/or spanned.

A close examination of the other curves in Fig. 5 for the portion in the accuracy range from H_2O zero/gain drift makes this conclusion more convincing. Given $T_c = 20$, in accuracy range, the portion from H_2O zero drift uncertainty is much greater (maximum 38% at –30 ºC) than that from H_2O gain drift uncertainty (maximum only 7% at 5 ºC). On average over the lower T_a range, the former is 27% and the latter only 4%. Further, given $T_c = 5$ ºC, in the accuracy range, the portion from H_2O gain drift uncertainty is even smaller (maximum only 3% at –5 ºC); in contrast, the portion from zero drift uncertainty is more major (one order higher, 30% at –30 ºC). On average over the lower T_a range, the minor gain drift uncertainty is 1.7%, and the major zero drift uncertainty is 17%. Both percentages underscore that the H_2O span procedure is reasonably unnecessary under cold/dry conditions, and, under such conditions, the H_2O zero procedure is the only necessary option to efficiently minimize H_2O measurement uncertainty in OPEC systems. This finding gives confidence in H_2O measurement accuracy to users who are worried about H_2O span procedures for infrared analyzers in the cold seasons when a dew point generator is not operational in the field (LI−COR Biosciences, 2004).
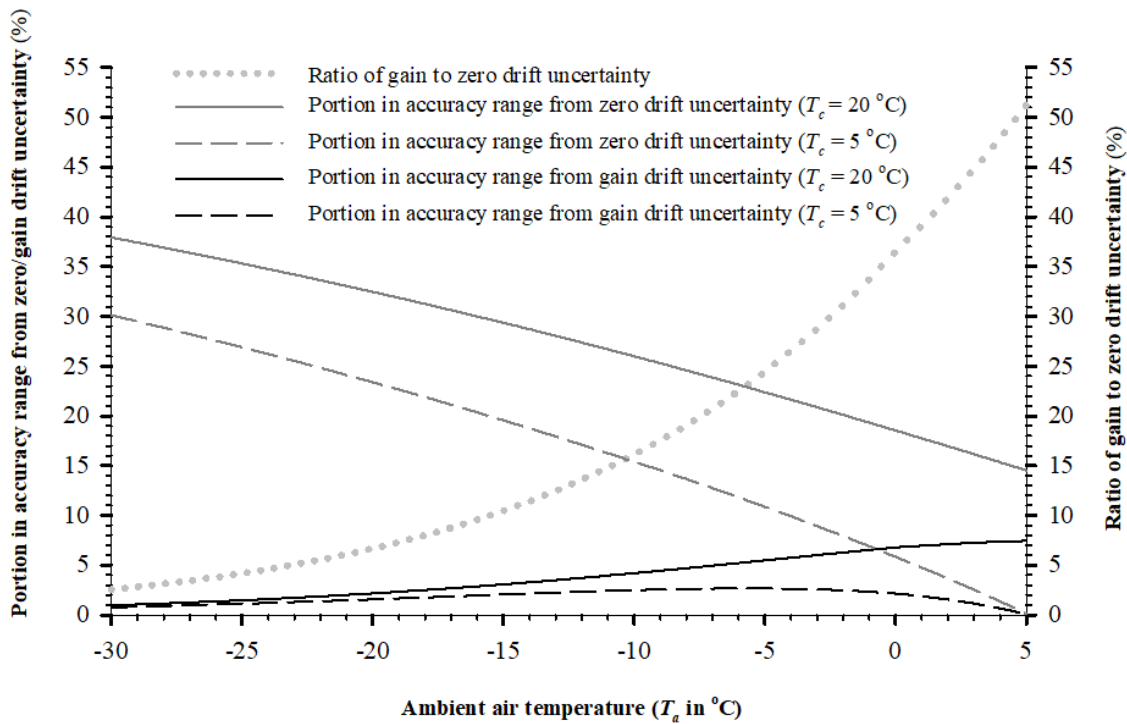
Figure 5. For a range of low T_a, the portion in the accuracy range from zero/gain drift uncertainty (left ordinate) and the ratio of gain to zero drift uncertainty (right ordinate). The curves are evaluated by Eqs. (18), (19), and (22) from measurement specifications for EC150 infrared CO_2−H_2O analyzers in open-path eddy-covariance flux systems over the T_a range from –30 to 5 ºC under atmospheric pressure of 101.325 kPa. T_c is the ambient air temperature at which an analyzer was calibrated, zeroed, and/or spanned.

6.3.3 H_2O zero procedure in cold and/or dry environments

620   In cold environments, although the non-operational H_2O span procedure is unnecessary, the H_2O zero procedure is asserted to be a prominently important option for minimizing the H_2O measurement uncertainty in OPEC systems. This procedure, although operational under freezing conditions, is still inconvenient for users when weather is very cold (e.g., when T_a is below –15 °C). If the field H_2O zero procedure is performed as needed above this T_a value, an OPEC system can be assumed to run at T_a with ±20 °C of T_c. Under this assumption, the poorest H_2O accuracy of ±0.066 gH_2O m^{-3} below 5 °C in Table 2

625   can be narrowed, through the H_2O zero procedure, by at least 22% to 0.051 gH_2O m^{-3} (assessed from data for Fig. 3a). Correspondingly, the relative accuracy range can be narrowed by the same percentage. The H_2O zero procedure can ensure both accuracy and relative accuracy of H_2O measurements in a cold environment (Fratini et al., 2014). In a dry environment, it plays the same role as in a cold environment, but it would be more convenient for users if warmer.

In a cold and/or dry environment, H_2O zero procedures that are undergone on a regular schedule would best

630   minimize the impact of zero drifts on measurements. Under such an environment, the automatic zero procedure for CO_2 and H_2O together in CPEC systems is an operational and efficient option to ensure and improve field CO_2 and H_2O measurement accuracies (Campbell Scientific Inc., 2021a; Zhou et al., 2021).

7 Discussion

An assessment methodology to evaluate the overall accuracies of field CO_2 and H_2O measurements from the infrared

635   analyzers in OPEC systems is developed using analyzer individual measurement uncertainties as specified using four uncertainty descriptors: zero drift, gain drift, sensitivity-to-CO_2/H_2O, and precision variability (Table 1). For the evaluation, these uncertainty descriptors are comprehensively composited into the accuracy model (2) and then formulated as a CO_2 accuracy equation (14) and an H_2O accuracy equation (22) (Sects. 3 to 5 and Appendix A). The assessment methodology, along with the model and the equations, present our development for the objective (Sects. 4.5 and 5.4).

7.1 Accuracy model

640

Accuracy model (2) composites the four measurement uncertainties (zero drift, gain drift, sensitivity-to-CO_2/H_2O, and precision variability) specified for analyzer performance as an accuracy range. This range is modeled as a simple addition of the four uncertainties. The simple addition is derived from our analysis assertion that the four measurement uncertainties interactionally or independently contribute to the accuracy range, but the contributions from the interactions inside any pair

645   of uncertainties are negligible since they are three orders smaller in magnitude than an individual contribution in the pair (Appendix A). This derived model is simple and applicable, paving an approach to the formulation of accuracy equations that are computable for evaluating the overall accuracies of field CO_2 and H_2O measurements from infrared analyzers in OPEC systems.

28

Additionally, included in the accuracy model, the four types of measurement uncertainties (zero drift, gain drift,
650   sensitivity-to-CO_2/H_2O, and precision variability) to specify the performance of infrared CO_2-H_2O analyzers for OPEC systems have been consistently used over last 20 years (LI−COR Biosciences, 2001, 2021a, 2021b; Campbell Scientific Inc., 2021). With the advancement of optical technologies, the measurement uncertainties for analyzer specifications are not expected to increase rather some current measurement uncertainties could be removed from the current specification list, even if not in the near future. If removed, the corresponding terms in the model could be easily removed, at which point, this
655   model would be adapted to the new set of specifications for infrared CO_2-H_2O analyzers.

7.2 Formulation of uncertainty terms in Model (2) for accuracy equations

In Sects. 4 and 5, each of the four uncertainty terms in accuracy model (2) is formulated as a computable sub-equation for CO_2 and H_2O, respectively (Eqs. 4, 7, 11, 13, 16, 18, 19, or 21). The accuracy model, whose terms are replaced with the formulated sub-equations for CO_2, becomes a CO_2 accuracy equation and, for H_2O, becomes an H_2O accuracy equation. In
660   the formulation, approximation is used for zero drift, gain drift, and sensitivity-to-CO_2/H_2O, while statistics are applied for precision variability.

For the zero/gain drift, although it is well known that the drift is influenced more by T_a if housing CO_2-H_2O accumulation is assumed to be minimized as insignificant under normal field maintenance (LI−COR Biosciences, 2021b; Campbell Scientific Inc., 2021b), the exact relationship of drift to T_a does not exist. Alternatively, the zero/gain drift
665   uncertainty is formulated by an approximation of drifts away from T_c linearly in proportion to the difference between T_a and T_c but within its maximum range over the operational range in T_a of OPEC systems (Eqs. 7, 11, 18, and 19). A drift uncertainty equation formulated through such an approximation is not an exact relationship of drift to T_a, but it does represent the drift trend, as influenced by T_a, to be understood by users. The accuracy from this equation at a given T_a is not exact either, but the maximum range over the full range, which is the most likelihood estimation, is most needed by users.

670   In fact, the H_2O accuracy as influenced by the linear trend of zero and gain drifts with the difference between T_a and T_c is more shadowed by the exponential trend of saturated H_2O density with T_a (Fig. 4b). Similarly, the CO_2 accuracy as influenced by the linear trend of zero and gain drifts with this difference is dominated by the CO_2 density of the ecosystem background with T_a, particularly in the low temperature range. Ultimately, the assumed linear trend does not play a dominant role in the accuracy trends of CO_2 and H_2O, which shows the merits of our methodology in the uses of atmospheric physics
675   and biological environment principles for the field data.

The sensitivity-to-CO_2/H_2O uncertainty can be formally formulated as Eq. (20) or (12), but, if directly used, this formulation would add an additional variable to the CO_2/H_2O accuracy equation. Equation (12) would add H_2O density (ρ_{H2O}) to the CO_2 accuracy equation, and Eq. (20) would add CO_2 density (ρ_{CO2}) to the H_2O accuracy equation. For either accuracy equation, the additional variable would complicate the uncertainty analysis. According to the ecosystem
680   environment background, the maximum range of sensitivity-to-CO_2/H_2O uncertainty is known and, compared to the

zero/gain drift as a major uncertainty (Table 1), this range is narrow (Table 1 and Eqs. 13 and 21). Therefore, the sensitivity-to-CO_2/H_2O uncertainty is approximated as Eq. (21) or (13). This approximation widens the accuracy range slightly, in a magnitude smaller than each of major uncertainties from the drifts at least in one order; however, it eliminates the need for ρ_{H2O} in the CO_2 accuracy equation and for ρ_{CO2} in the H_2O accuracy equation, which makes the equations easily applicable.

685   Precision uncertainty is statistically formulated as Eq. (4) for CO_2 and Eq. (16) for H_2O. This formulation is a common practice based on statistical methods (Hoel, 1984).

7.3 Use of relative accuracy for infrared analyzer specifications

Relative accuracy is often used concurrently with accuracy to specify sensor measurement performance. The accuracy is the numerator of relative accuracy whose denominator is the true value of a measured variable. When evaluated for the
690   applications of OPEC systems in ecosystems, CO_2 accuracy magnitude is small in a range within one order (0.39 ~ 1.21 $mgCO_2$ m^{-3}, data for Fig. 2a), and so is H_2O accuracy (0.04 ~ 0.10 gH_2O m^{-3}, data for Fig. 3a). In ecosystems, CO_2 is naturally high, as compared to its accuracy magnitude, and does not change much in terms of a magnitude order (e.g., no more than one order from 600 to 1,600 gH_2O m^{-3}, assumed in this study). However, unlike CO_2, H_2O naturally changes in its amount dramatically across at least three orders in magnitude (e.g., at 101.325 kPa, from 0.03 gH_2O m^{-3} when RH is 10% at
695   –30 ºC to 40 gH_2O m^{-3} when dew point temperature is 35 ºC at the highest as reported by National Weather Service (2021); under drier conditions, the H_2O amount could be even lower). Because, in ecosystems, CO_2 changes differently than H_2O in amount across magnitude orders, the relative accuracy behaviors in CO_2 differ from H_2O (Figs. 2b and 3b).

7.3.1 CO_2 relative accuracy

Because of the small CO_2 accuracy magnitude relative to the natural CO_2 amount in ecosystems, the CO_2 relative accuracy
700   magnitude varies within a narrow range of 0.07 to 0.19% (Sect. 4.5.2). If the relative accuracy is used, either a range of 0.07 − 0.19% or an inequality of ≤ 0.19% can be specified as the CO_2 relative accuracy magnitude for field CO_2 measurements. Both range and inequality would be equivalently perceived by users to be a fair performance of OPEC systems. For simplicity, our study with the OPEC systems can be specified for their CO_2 relative accuracy to be ±0.19%.

7.3.2 H_2O relative accuracy

705   Although the H_2O accuracy magnitude is also small, the "relatively" great change in natural air H_2O across several magnitude orders in ecosystems results in a much wider range of the H_2O relative accuracy magnitude, from 0.23% at maximum air moisture to 96% when RH is 20% at –30 ºC (Fig. 3b and Sect. 5.4.2). H_2O relative accuracy can be much greater under dry conditions at low T_a (e.g., 192% for air when RH is 10% at –30 ºC). Accordingly, if the relative accuracy is used, either a range of 0.23 − 192% or an inequality of ≤ 192% can be specified as the H_2O relative accuracy magnitude for

710   field H_2O measurements. Either $0.23 - 192\%$ or $\leq 192\%$ could be perceived by users intrinsically as poor measurement performance of the infrared analyzers, although either specification is conditionally right for fair H_2O measurement.

Apparently, the relative accuracy for H_2O measurements in ecosystems is not intrinsically interpretable by users to correctly perceive the performance of OPEC systems. Instead, if H_2O relative accuracy is unconditionally specified just in an inequity of $\leq 192\%$, it could easily mislead users to wrongly assess the performance of OPEC systems as unacceptable for

715   H_2O measurements, although this performance of OPEC systems is fair for air when RH is 10% at –30 ºC. Therefore, H_2O relative accuracy is not recommended to be used for specification of infrared analyzers for H_2O measurement performance. If this descriptor is used, the H_2O relative accuracy under a standard condition should be specified. This condition may be defined as saturated air at 35 ºC (i.e., the highest natural dew point (National Weather Service, 2021)) under normal P of 101.325 kPa (Wright et al., 2003). For our study case, under such a standard condition, the H_2O relative accuracy can be

720   specified within $\pm 0.18\%$ after manufacturing calibration (data for Fig. 3b).

8 Conclusions

The accuracy of field CO_2/H_2O measurements from the infrared analyzers in OPEC systems can be defined as a maximum range of composited measurement uncertainty from the specified sources: zero drift, gain drift, sensitivity-to-CO_2/H_2O, and precision variability (Table 1), all of which are included in the system specifications for CO2-H2O analyzers currently used

725   in field OPEC systems. The specified uncertainties interactionally or independently contribute to the overall uncertainty. Fortunately, the interactions between component uncertainties in each pair is three orders smaller than either component individually (Appendix A). Therefore, these specified uncertainties can be simply added together as the accuracy range in a general CO_2/H_2O accuracy model for OPEC systems (Model 2). Based on statistics, bio-environment, and approximation, the specification descriptors of the infrared analyzers in OPEC systems are incorporated into the model terms to formulate

730   the CO_2 accuracy equation (14) and the H_2O accuracy equation (22), both of which are computable to evaluate corresponding CO_2 and H_2O accuracies. For EC150 infrared analyzers used in the OPEC systems over their operational range in T_a at the standard P of 101.325 kPa (Figs. 2 and 3 and Table 2), the CO_2 accuracy can be specified as ± 1.21 mgCO2 m^{-3} (relatively within $\pm 0.19\%$, Fig. 2) and H_2O accuracy as ± 0.10 gH2O m^{-3} (relatively within $\pm 0.18\%$ for saturated air at 35 ºC at the standard P, Fig. 3).

735   Both accuracy equations are not only applicable for further uncertainty estimation for CO_2 and H_2O fluxes due to measurement uncertainties of CO_2 and H_2O density (Eqs. 27 and 28) and the error/uncertainty analyses in CO_2 and H_2O data applications (e.g., Eq. 29), but they also may be used as a rationale to assess and guide field maintenance on infrared analyzers. Combining Eq. (14) as shown in Fig. 2a with Eqs. (7) and (11) as shown in Fig. 4a guides users to adjust the CO_2 zero and gain drifts, through the corresponding zero and span procedures, near a T_a value that minimizes the T_a departures,

740   on average, during the period of interest if this period were not under extreme and hazard conditions (Fratini et al., 2014). As assessed on atmospheric background, the procedures can narrow the maximum CO_2 accuracy range by 40%, from ± 1.21 to

± 0.72 mgCO$_2$ m^{-3}, and thereby greatly improve the CO$_2$ measurement accuracies with these regular CO$_2$ zero and span procedures.

Equation (22) as shown in Fig. 3a, along with Eqs. (18) and (19) as shown in Fig. 4b, present users with a rationale
745   to adjust the H$_2$O zero drift of analyzers in the same technique as for CO$_2$, but the H$_2$O gain drift under hot and humid environments needs more attention (see the right portion above T_c in Figs. 3a and 4b); under cold and/or dry environments, it needs no further concern (see the left portion below 0 ºC in Fig. 4b). In a T_a range above 5 ºC, the maximum H$_2$O accuracy range of ± 0.10 gH$_2$O m^{-3} can be narrowed by 30% to ± 0.07 gH$_2$O m^{-3} if both H$_2$O zero and span procedures are performed as necessary. In a T_a range below 5 ºC, the H$_2$O zero procedure alone can narrow the maximum H$_2$O accuracy range of
750   ± 0.076 gH$_2$O m^{-3} by 22%, to ± 0.051 gH$_2$O m^{-3}. Under cold environmental conditions, the H$_2$O span procedure is found to be unnecessary (Fig. 5), and the H$_2$O zero procedure is proposed as the only, and prominently efficient, option to minimize H$_2$O measurement uncertainty in OPEC systems. This procedure plays the same role under dry conditions. Under cold and/or dry environments, the zero procedure for CO$_2$ and H$_2$O together would be a practical and efficient option to not only warrant, but also to improve, measurement accuracy. In a cold environment, adjusting the H$_2$O gain drift is impractical because of the
755   failure of a dew point generator under freezing conditions.

Additionally, as a specification descriptor for OPEC systems used in ecosystems, relative accuracy is applicable for CO$_2$ instead of H$_2$O measurements. A small range in the CO$_2$ relative accuracy can be perceived intuitively by users as normal. In contrast, without specifying the condition of air moisture, a large range in H$_2$O relative accuracy under cold and/or dry conditions (e.g., 100%) can easily mislead users to an incorrect conclusion in interpretation of H$_2$O measurement
760   reliability, although, it is the best achievement of the modern infrared analyzers under such conditions. The authors suggest to conditionally define H$_2$O relative accuracy at 35 °C dew point (i.e., 39.66 gH$_2$O m^{-3} at 101.352 kPa). Ultimately, this study provides some scientific bases to the flux community in specifying the accuracy of CO$_2$−H$_2$O measurements from infrared analyzers in OPEC systems although only one model of EC150 is used for this study.

Appendix A: Derivation of accuracy model for infrared CO$_2$−H$_2$O analyzers

765   As defined in the Introduction, the measurement accuracy of infrared CO$_2$−H$_2$O analyzers is a range of the difference between the true α density (ρ_{aT}, where α can be either H$_2$O or CO$_2$) and measured α density (ρ_a) by the analyzer. The difference is denoted by $\Delta \rho_a$, given by Eq. (1) in Sect. 3. Analyzer performance uncertainties contribute to this range, as specified in the four descriptors: zero drift, gain drift, cross-sensitivity, and precision (LI−COR Biosciences, 2021b; Campbell Scientific Inc., 2021b).

770   According to the definitions in Sect. 2, zero drift uncertainty ($\Delta \rho_\alpha^z$) is independent of ρ_{aT} value and gain trend related to analyzer response; so, too, is cross-sensitivity uncertainty ($\Delta \rho_\alpha^s$), which depends upon the amount of background H$_2$O in the measured air if α is CO$_2$, and upon the amount of background CO$_2$ in the measured air if α is H$_2$O. In the case that

both gain drift and precision uncertainties are zero, $\Delta\rho_\alpha^z$ and $\Delta\rho_\alpha^s$ are simply additive to any true value as a measured value, including zero drift and cross-sensitivity uncertainties (ρ_{α_zs})

$$\rho_{\alpha\_zs} = \rho_{\alpha T} + \Delta\rho_\alpha^z + \Delta\rho_\alpha^s, \qquad\qquad (A1)$$

where subscript z indicates zero drift uncertainty included in the measured value, and subscript s indicates cross-sensitivity uncertainty included in the measured value. During the measurement process, while zero is drifting and cross-sensitivity is active, if gain also drifts, then the gain drift interacts with the zero drift and the cross-sensitivity. This is because ρ_{α_zs} is a linear factor for this gain drift (see the cells in gain-drift row and value columns in Table 1) that is added to ρ_{α_zs} as a measured value additionally including gain drift uncertainty (ρ_{α_zsg}, where subscript g indicates gain drift uncertainty included in the measured value), given by

$$\rho_{a\_zsg} = \rho_{\alpha\_zs} + \delta_{\alpha\_g}\rho_{\alpha\_zs}, \qquad\qquad (A2)$$

where δ_{α_g} is gain drift percentage ($\delta_{CO2\_g} = 0.10\%$ and $\delta_{H2O\_g} = 0.30\%$, Table 1). Substituting ρ_{α_zs} in this equation with Eq. (A1) leads to

$$\rho_{a\_zsg} = \rho_{\alpha T} + \Delta\rho_\alpha^z + \Delta\rho_\alpha^s + \delta_{\alpha\_g}\rho_{\alpha T} + \delta_{\alpha\_g}\Delta\rho_\alpha^z + \delta_{\alpha\_g}\Delta\rho_\alpha^s \ . \qquad\qquad (A3)$$

In this equation, $\delta_{\alpha\_g}\Delta\rho_\alpha^z$ is the zero-gain interaction, and $\delta_{\alpha\_g}\Delta\rho_\alpha^s$ is the sensitivity-gain interaction. In magnitude, the former is three orders smaller than either zero drift uncertainty ($\Delta\rho_\alpha^z$) or gain drift uncertainty ($\delta_{\alpha\_g}\rho_{\alpha T}$). The sensitivity-gain interaction is three orders smaller than either cross-sensitivity uncertainty ($\Delta\rho_\alpha^s$) or gain drift uncertainty. Therefore, both interactions are relatively small and can be reasonably dropped. As a result, Eq. (A3) can be approximated and rearranged as:

$$\begin{aligned}\rho_{a\_zsg} &\approx \rho_{\alpha T} + \Delta\rho_\alpha^z + \delta_{\alpha\_g}\rho_{\alpha T} + \Delta\rho_\alpha^s \\ &= \rho_{\alpha T} + \Delta\rho_\alpha^z + \Delta\rho_\alpha^g + \Delta\rho_\alpha^s\end{aligned}, \qquad\qquad (A4)$$

where $\Delta\rho_\alpha^g$ is gain drift uncertainty. Any measured value has random error (i.e., precision uncertainty) independent of $\rho_{\alpha T}$ in value (ISO, 2012). Therefore, ρ_{α_zsg} plus precision uncertainty ($\Delta\rho_\alpha^p$) is the measured value including all uncertainties (ρ_a), given by

$$\rho_a = \rho_{a\_zsg} + \Delta\rho_\alpha^p . \qquad\qquad (A5)$$

The insertion of Eq. (A4) into this equation leads to

$$\rho_a - \rho_{\alpha T} = \Delta\rho_\alpha^z + \Delta\rho_\alpha^g + \Delta\rho_\alpha^s + \Delta\rho_\alpha^p . \qquad\qquad (A6)$$

This equation holds

$$\Delta\rho_a \le \left|\Delta\rho_\alpha^z\right| + \left|\Delta\rho_\alpha^g\right| + \left|\Delta\rho_\alpha^s\right| + \left|\Delta\rho_\alpha^p\right|. \qquad\qquad (A7)$$

The range of the right side of this equation is wider than the measurement uncertainty from all measurement uncertainty sources and the difference of ρ_α minus $\rho_{\alpha T}$ (i.e., $\Delta\rho_\alpha$). Using this range, the measurement accuracy is defined in Model (2) in Sect. 3.

Appendix B: Water vapor density from ambient air temperature, relative humidity, and atmospheric pressure

Given ambient air temperature (T_a in °C) and atmospheric pressure (P in kPa), air has a limited capacity to hold an amount of water vapor (Wallace and Hobbs, 2006). This limited capacity is described in terms of saturation water vapor density (ρ_s in gH$_2$O m^{-3}) for moist air, given through the Clausius–Clapeyron equation (Sonntag, 1990; Wallace and Hobbs, 2006)

$$\rho_s(T_a,P) = \frac{0.6112 f(P)}{R_v(273.15+T_a)} \begin{cases} \exp(\dfrac{17.62 T_a}{T_a+243.12}) & T_a \geq 0 \\[2mm] \exp(\dfrac{22.46 T_a}{T_a+272.62}) & T_a < 0 \end{cases}, \tag{B1}$$

where R_v is the gas constant for water vapor (4.61495×10^{-4} kPa m^3 K^{-1} gH$_2$O^{-1}), and $f(P)$ is an enhancement factor for moist air, being a function of P: $f(P) = 1.0016 + 3.15 \times 10^{-5} P - 0.0074 P^{-1}$. At relative humidity (RH in %), the water vapor density [$\rho_{H_2O}^{RH}(T_a,P)$ in gH$_2$O m^{-3}] is

$$\rho_{H_2O}^{RH}(T_a,P) = RH\rho_s(T_a,P). \tag{B2}$$

This equation, along with Eq. (B1), is used to calculate $\rho_{H_2O}^{RH}$ used in Fig. 3 in Sect. 5 and Figs. 4b and 5 in Sect. 6.3.

Appendix C: The relationship of measured to true covariance to of vertical wind speed with CO₂, H₂O, and air temperature

For open-path eddy-covariance systems, the computation of CO$_2$/H$_2$O flux between ecosystems and the atmosphere starts from covariance of 3-D wind with a CO$_2$/H$_2$O density. Same as in Eqs. (1) and (2), α is used as a subscript of ρ to represent either CO$_2$ or H$_2$O and subscript T is used to indicates "true". According to Eq. (1), a measured α density (ρ_α) can be expressed as

$$\rho_\alpha = \rho_{\alpha T} + \Delta\rho_\alpha, \tag{C1}$$

where $\rho_{\alpha T}$ denotes true α density and $\Delta\rho_\alpha$ is measurement uncertainty of ρ_α. The covariance of vertical wind speed (w) with measured α density is given by

$$\overline{w'\rho_\alpha'} = \frac{1}{n}\sum_{i=1}^{n}(w_i-\bar{w})(\rho_\alpha-\bar{\rho}_\alpha), \tag{C2}$$

where n is the sample number over an averaging interval (e.g., 36,000 over an hour interval if w and ρ_α are measured at 10 Hz), the overbar is an averaging operator, and prime denotes the fluctuation of a variable away from its mean (e.g., $w_i' = w_i - \overline{w}$). Without considering the measurement error of w for this study topic, submitting Eq. (C1) into (C2) leads to

$$\overline{w'\rho_\alpha'} = \frac{1}{n}\sum_{i=1}^{n}(w_i - \overline{w})\left[\rho_{\alpha Ti} + \Delta\rho_{\alpha i} - \overline{(\rho_{\alpha Ti} + \Delta\rho_{\alpha i})}\right]$$

$$= \frac{1}{n}\sum_{i=1}^{n}(w_i - \overline{w})(\rho_{\alpha Ti} - \overline{\rho}_{\alpha T}) + \frac{1}{n}\sum_{i=1}^{n}(w_i - \overline{w})(\Delta\rho_{\alpha i} - \Delta\overline{\rho}_\alpha)$$

825 (C3)

Over an hour interval, the systematic error components inside terms $\Delta\rho_{\alpha i}$ and $\Delta\overline{\rho}_\alpha$ are not only constant, but also equal. Accordingly, the systematic errors inside the term $\Delta\rho_{\alpha i} - \Delta\overline{\rho}_\alpha$ are cancelled out (Richardson et al., 2012). In essence, this term is a random error whose distribution generally is assumed to be normal. As such, the expected mean of $\Delta\rho_{\alpha i} - \Delta\overline{\rho}_\alpha$ is zero (Hoel, 1984). The correlation of w with a random variable with an expected zero mean tends to be zero, particularly for

830 a large sample number of 36,000 under discussion (Snedecor and Cochran, 1989). Accordingly, the second term in the second line of Eq. (C3) is zero. Therefore, the covariance of w with measured α density is equal to the covariance of w with true α density, given by

$$\overline{w'\rho_\alpha'} = \overline{w'\rho_{\alpha T}'} \; .$$

(C4)

If w from a sonic anemometer and ρ_α from an infrared analyzer are not measured through spatial and temporal

835 synchronization, the values of covariance of w with ρ_α in the different lags of measurement (hereafter referred to as the lagged covariance) are computed to find the maximum covariance as if w and ρ_α were measured at the same time in the same space (Moncrieff et al., 1997; Ibrom et al., 2007). Each lagged covariance can be expressed as $\overline{w'\rho_{\alpha l}'}$, where subscript l is the index for a lag number. If $l = 0$, w_i and $\rho_{\alpha 0 i}$ were measured at the same time. If $l = -1$, w_i was measured one measurement interval (i.e., 100 ms for 10-Hz measurements) later than $\rho_{\alpha(-1)i}$ whereas w_i was measured one measurement interval earlier

840 than and $\rho_{\alpha 1 i}$ if $l = 1$. The index l can be $-k$ to k where k is a positive integer, including 0, to represent the maximum number of the lags that is optional to users. Therefore, given l from $-k$ to k, the number of values for $\overline{w'\rho_{\alpha l}'}$ is $2k+1$. Using the same approach to Eq. (C4), $\overline{w'\rho_{\alpha l}'} = \overline{w'\rho_{\alpha Tl}'}$ can be proved.

The lagged covariance values for $\overline{u'\rho_{\alpha l}'}$ and $\overline{v'\rho_{\alpha l}'}$ (l is $-k$, $-k+1$, …,0, …, or k) are also computed for each lag where, in the sonic anemometer coordinate system, u is the wind speed in the x direction and v is the wind speed in the y direction.

845 Both $\overline{u'\rho_{\alpha l}'} = \overline{u'\rho_{\alpha Tl}'}$ and are also can be proved in the same way for Eq. (C4). Given the rotation angles from $\overline{u}, \overline{v}, \overline{w}, \overline{u'^2}, \overline{v'^2}, \overline{v'^2}, \overline{u'v'}, \overline{u'w'}$, and $\overline{v'w'}$ (Tanner and Thurtell, 1960), each set of $\overline{u'\rho_{\alpha l}'}, \overline{v'\rho_{\alpha l}'}$, and $\overline{w'\rho_{\alpha l}'}$ are rotated to be

35

$\overline{\left(u'\rho'_{\alpha l}\right)}_r$, $\overline{\left(v'\rho'_{\alpha l}\right)}_r$, and $\overline{\left(w'\rho'_{\alpha l}\right)}_r$, respectively. In the rotation process, ρ_α is not additionally involved. Because $\rho'_{\alpha l}$ inside the covariance is a scaler rather than vector variable, the rotation would not be influenced by $\overline{\rho}_{\alpha l}$ and $\overline{\rho^2_{\alpha l}}$ as by the three means and three variance values of 3-D wind components (Tanner and Thurtell, 1960). Therefore, the covariance values rotated from $\overline{u'\rho'_{\alpha l}}, \overline{v'\rho'_{\alpha l}}$, and $\overline{w'\rho'_{\alpha l}}$ are correspondingly equal to those rotated from $\overline{u'\rho'_{\alpha Tl}}, \overline{v'\rho'_{\alpha Tl}}$, and $\overline{w'\rho'_{\alpha Tl}}$. Accordingly,

$$\overline{\left(w'\rho'_{\alpha l}\right)}_r = \overline{\left(w'\rho'_{\alpha Tl}\right)}_r . \tag{C5}$$

Therefore, the maximum covariance in magnitude among $\overline{\left(w'\rho'_{\alpha l}\right)}_r$ (l from $-k$ to k) $[\overline{\left(w'\rho'_{\alpha}\right)}_{rm}]$ is equal to the maximum in magnitude among $\overline{\left(w'\rho'_{\alpha Tl}\right)}_r$ $[\overline{\left(w'\rho'_{\alpha T}\right)}_{rm}]$ (Moncrieff et al., 1997; Ibrom et al., 2007), given by

$$\overline{\left(w'\rho'_{\alpha}\right)}_{rm} = \overline{\left(w'\rho'_{\alpha T}\right)}_{rm} \tag{C6}$$

Multiplying the frequency correction factor (f_c) on the both sides of this equation to correct the low- and high-frequency loss (Moore, 1986; Massman, 2000; van Dijk, 2002) leads to

$$f_c\overline{\left(w'\rho'_{\alpha}\right)}_{rm} = f_c\overline{\left(w'\rho'_{\alpha T}\right)}_{rm} . \tag{C7}$$

f_c is integrated from the cospectrum of w with T_a (air temperature, as a proxy of $\rho_{\alpha T}$ for spectrum representation) and the transfer functions of high-frequency loss for w, ρ_α (Moore, 1986; van Dijk, 2002), and low-frequency loss for averaging $w'\rho'_\alpha$ (Massman, 2000). Over the integration, ρ_α is not involved through cospectum and transfer functions, either. If the left-side term of Eq. (C7) is expressed as $\overline{\left(w'\rho'_\alpha\right)}_{rmf}$ and the right-side one as $\overline{\left(w'\rho'_{\alpha T}\right)}_{rmf}$, Eq. (C7) leads to

$$\overline{\left(w'\rho'_\alpha\right)}_{rmf} = \overline{\left(w'\rho'_{\alpha T}\right)}_{rmf} , \tag{C8}$$

where subscript rmf indicates the covariance was corrected through coordinate rotations (r), lag maximization (m), and low- and high-frequency (f) corrections. Equation (C8) shows the covariance of w with measured ρ_α is equal to its counterpart with true ρ_α even after these corrections before used to calculate the α flux through WPL correction (Webb et al., 1982).

For the covariance of w with T_a, the same conclusion can be derived, given by

$$\overline{\left(w'T'_a\right)}_{rmf} = \overline{\left(w'T'_{aT}\right)}_{rmf} \tag{C9}$$

Assume w to be true value for this study topic, through WPL correction, $\overline{\left(w'\rho'_\alpha\right)}_{rmf}$ and $\overline{\left(w'T'_a\right)}_{rmf}$ can be used to derive an analytical equation for α flux from ρ_α with an error as ranged by its accuracy and T_a with an errors whereas $\overline{\left(w'\rho'_{\alpha T}\right)}_{rmf}$ and

870　$\overline{\left(w'T'_{aT}\right)}_{rmf}$ can be used to derive an analytical equation for α flux from ρ_{aT} and T_{aT}, both of which theoretically do not include errors. The comparison of both analytical equations can demonstrate the partial effects of $\Delta\rho_\alpha$ on uncertainty of hourly α flux (see Sect. 6.2).

Author Contributions

XZ, BY, TG, and NZ contributed equally to this this work; YL, FY, and YA discussed the points of this study topic and
875　made comments on the manuscript; JZ led the team.

Competing interest

XZ, BY, and YL have affiliation with Campbell Scientific Incorporation, which is the manufacturer of the example model EC150 of infrared CO_2-H_2O analyzers. The authors declare that they have no conflict of interest.

References

890　AmeriFlux: Data Variables, Lawrence Berkeley National Laboratory, http://ameriflux.lbl.gov/data/aboutdata/data-variables/, 1–12 pp., 2018.

Andreas, E. L.: The effects of volume averaging on spectral measured with a Lyman-Alpha hygrometer, 20: 467–475, https://doi.org/10.1175/1520-0450(1981)020<0467:TEOVAO>2.0.CO;2, 1981.

Anthoni, P. M., Law, B. E., and Unworth, M. H.: Carbon and water vapor exchange of an open-canopied ponderosa pine
895　ecosystem, Agricultural Forest Meteorology, 95: 151–168, https://doi.org/10.1016/S0168-1923(99)00029-5, 1999.

Anthoni, P. M., Freibauer, A., Kolle, O., and Schulze, E. D.: Winter wheat carbon exchange in Thurngia, Germany, Agricultural Forest Meteorology, 121: 55–67, https://doi.org/10.1016/S0168-1923(03)00162-X, 2004.

Aubinet, M., Vesala, T., and Papale, D. (eds): Eddy Covariance: A Practice Guide to Measurement and Data Analysis, Springer, New York, 438 p, https://doi.org/10.1007/978-94-007-2351-1, 2012.

900   Buck, A. L.: New equations for computing vapor pressure and enhancement factor, Journal of Applied Meteorology, 20: 1527–1532, https://doi.org/10.1175/1520-0450(1981)020<1527:NEFCVP>2.0.CO;2, 1981.

Burba, G., Anderson, T., and Komissarov, A.: Accounting for spectroscopic effects in laser-based open-path eddy covariance flux measurements, Global Change Biology, 25, 2189-2202, DOI: 10.1111/gcb.14614, 2019.   Burden, R. L., Faires, J. D., and Burden, A.M: Numerical Analysis, 10th ed., Gengage Learning, Boston, 896 p., 2016.

905   Campbell Scientific Inc.: CPEC300/306/310 CO_2/H_2O Closed-Path Eddy-Covariance Systems, Revision 08/21, Logan, UT, USA, 92 p., 2021a.

Campbell Scientific Inc.: EC150 CO_2/H_2O Open-Path Gas Analyzer, Revision 09/21, Logan, UT, USA, 41 p., 2021b.

Csavina, J., Roberti, J. A., Taylor, J. R., and Loescher, H. W.: Traceable measurements and calibration: A primer on uncertainty analysis, Ecosphere, 8(2): e01683, http://doi.wiley.com/10.1002/ecs2.1683, 2017.

910   Finnigan, J. An introduction to flux measurements. Ecological Applications, 18(6):1340–1350, https://doi.org/10.1890/07-2105.1, 2008.

Flanaganm L. B. and Johnson, B. G.: Interacting effects of temperature, soil moisture, and plant biomass production on ecosystem respiration in a north temperate grassland. Agricultral and Forest Meteorology, 130: 237–253, https://doi.org/10.1016/j.agrformet.2005.04.002, 2005.

915   Foken, T.: The energy ballance closure problem: An overview, Ecological Applications, 18(6), 1351–1367, https://doi.org/10.1890/06-0922.1, 2008.

Foken, T., Göckede, M., Mauder, M., Mahrt, L., Amiro, B.D., and Munger, J. W.: Post-field data quality control, In: Handbook of Micrometeorology: A Guide for Surface Flux Measurement and Analysis, edited by Lee, X., Massman, W., and Law B., 181–208, Kluwer Academic Publishers, New York, 2004.

920   Foken, T., Leuning, R., Onley, S. R., Mauder, M., Aubinet, M.: Correction and data quality control, In: Eddy Covariance: A Practice Guide to Measurement and Data Analysis, edited by Aubinet, M., Vesala, T., and Papale D., 85–131, Springer, New York, https://doi.org/10.1007/978-94-007-2351-1_4, 2012.

Fratini, G., McDermitt, D. K., and Papale, D.: Eddy-covariance flux errors due to biases in gas concentration measurements: Origins, quantification and correction, Biogeisciences, 11: 1037-1051, 2014

925   Global Monitoring Laboratory: Trends in Atmospheric Carbon Dioxide. Accessed October 01, 2021, https://www.esrl.noaa.gov/gmd/ccgg/trends/weekly.html, 2021.

Goulden, M. L., Munger, J. W., Fan, S. M., Daube, B. C., and Wofsy, S. C.: Measurements of carbon sequstration by long-term eddy covariance: Method and a critical ecaluation of accuracy. Global Change Biology, 2: 169–181, https://doi.org/10.1111/j.1365-2486.1996.tb00070.x, 1996.

38

930 Hill, T., Chocholek, M., and Clement, R.: The case for increasing the statistical power of eddy covariance ecosystem study, where and how, Global Change Biology, 23: 2154–2165, https://doi.org/10.1111/gcb.13547, 2017.

Hoel, P. G.: Introduction to Mathematical Statistics, 5th ed, John Wiley & Son, New York, 435 pp, 1984.

Horst, T. W.: On frequency response corrections for eddy covariance flux measurements: Research note, Boundary-Layer Meteorology, 94: 517–520, https://doi.org/10.1023/A:1002427517744, 2000.

935 Ibrom, A., Dellwik, E., Flyvbjerg, H., Jensen, N. O., and Pilegaard, K.: Strong low-pass filtering effects on water vapour flux measurements with closed-path eddy correlation systems, Agr. Forest Meteorol., 147, 140–156, https://doi.org/10.1016/j.agrformet.2007.07.007, 2007.

ISO: Accuracy (trueness and precision) of measurement methods and results — Part 1: General principles and definitions, ISO 5725-1, 1994 (reviewed in 2012), International Organization for Standardization, Geneva, Switzerland, 17 pp.,
940 2012.

Joint Committee for Guides in Metrology: Evaluation of measurement data: Guide to the expression of uncertainty in measurement, 1st ed, Research Triangle Park, NC, USA: JCGM Member Organization, 2008.

Kaimal, J. C. and Haugen, D. J.: Some errors in the measurement of Reynold stress, Journal of Applied Meteorology, 8: 160−162, http://www.jstor.org/stable/26174564, 1969.

945 Katul, G., Gava, D., Poggi, D., Albertson, J., Mahrt, L.: Satationary, homogeneity, and ergodicity in canopy turbulence, In: Handbook of Micrometeology: A Guide for Surface Flux Measurement and Analysis, edited by Lee, X, Massman, W., and Law, B., 161–180, Kluwer Academic Publishers, Dordrecht, 2004.

Laubach, J., and McNaughton, K. G.: A spectrum-independent procedure for correcting eddy fluxes measured with separated sensors, Boundary-Layer Meteorology, 89: 445−467, https://doi.org/10.1023/A:1001759903058, 1998.

950 Lee, X. and Massman, W. J.: A Perspective on thirty years of the Webb, Pearman and Leuning density corrections, Boundary-Layer Meteorology, 139: 37–59, https://doi.org/10.1007/s10546-010-9575-z, 2011.

Lee, X., Fuentes, J. D., Staebler, R. M., Neumann, H. H.: Long-term observation of the atmospheric exchange of CO_2 with a temperate deciduous forest in southern Ontario, Canada, Journal of Geophysical Research Atmospheres, 104: 15975−15984, https://doi.org/10.1029/1999JD900227, 1999.

955 Lenschow, D. H., Mann, J., and Kristensen, L.: How long is long enough when measuring flues and other turbulence statistics?, Journal of Atmospheric and Oceanic Technology, 11(3): 661−673, https://doi.org/10.1175/1520-0426(1994)011<0661:HLILEW>2.0.CO;2, 1994.

LI−COR Biosciences: LI−610 Portable Dew Point Generator: Instruction Manual, 3−1~20, Lincoln, NE, USA, 2004.

LI−COR Biosciences: LI−7200RS Closed CO_2/H_2O Gas Analyzer: Instruction Manual, p. 1−1~H−4, Lincoln, NE, USA,
960 2021a.

LI−COR Biosciences: LI−7500 CO_2/H_2O Analyzer: Instruction Manual, p. 1−1 ~ D35., Lincoln, NE, USA, 2001.

LI−COR Biosciences: Using the LI−7500DS Open Path CO_2/H_2O Gas Analyzer and the SmartFlux 3 Systems: Instruction Manual, 4−1~11 and 8−1~9, Lincoln, NE, USA, 2021b.

Massman, W. J.: A simple method for estimating frequency response corrections for eddy covariance systems, Agricultural and Forest Meteorology, 104: 185−198, https://doi.org/10.1016/S0168-1923(00)00164-7, 2000.

McDermitt, D. K., Welles, J. M., and Eckles, R. D.: Effects of temperature, pressure and water vapor on gas phase infrared absorption by CO_2, LI−COR Application Note #116, 5 p., 1993.

Moncrieff, J. B., Massheder, J. M., de Bruin, H., Elbers, J., Friborg, T., Heusinkveld, B., Kabat, P., Scott, S., Soegaard, H., and Verhoef, A.: A system to measure surface fluxes of momentum, sensible heat, water vapour and carbon dioxide, J. Hydrol., 188-189, 589–611, https://doi.org/doi:10.1016/S0022-1694(96)03194-0, 1997.

Moore, C. J.: Frequency response corrections for eddy correlation systems, Boundary-Layer Meteorology, 37, 17–35, https//doi.org/10.1007/BF00122754, 1986.

Munger, W. J., Loescher, H. W., and Luo, H.: Measurement, tower, and site design considerations, In: Eddy Covariance: A Practice Guide to Measurement and Data Analysis, edited by Aubinet, M., Vesala, T., and Papale D., 85–131, Springer, New York, https://doi.org/10.1007/978-94-007-2351-1_2, 2012.

National Weather Service: Fast Facts, National Oceanic and Atmospheric Administration, Accessed October 01, 2021, https://www.weather.gov, 2021.

Ohkubo, S., Kosugi, Y., Takanashi, S., Matsuo, N., Tani, M., and Nik, A. R.: Vertical profiles and storage fluxes of CO_2, heat and water in a tropical rainforest at Pasoh, Peninsular Malaysia, Tellus, 60B: 569–582, https://doi.org/10.1111/j.1600-0889.2008.00367.x, 2018.

Rannik, Ü. and Vesala, T.: Autoregressive filtering versus linear detrending in estimation of fluxes by the eddy covariance method, Boundary-Layer Meteorology, 91: 259–280, https://doi.org/10.1023/A:1001840416858, 1999.

Richardson, A.D., Aubinet, M., Barr, A. G., Hollinger, D. Y., Ibrom, A, Lasslop, G., and Reichstein, M.: Uncetryaity quantification, In: Eddy Covariance: A Practice Guide to Measurement and Data Analysis, edited by Aubinet, M., Vesala, T., and Papale D., 85–131, Springer, New York, https://doi.org/10.1007/978-94-007-2351-1_7, 2012.

Richardson, A.D. and Hollinger, D. Y.: A method to estimate the additional uncerttainty in gap-filled NEE resulting from long gaps in the CO2 flux record. Agricultral and Forest Meteorology, 130: 237–253, https://doi.org/10.1016/j.agrformet.2007.06.004, 2007.

Snedecor, G. W and Cochran, W. G. (Eds.): Statistical Methods (8th ed), Iowa State University Press, Ames, IA, USA, 502 p., 1989.

Sonntag, D.: Important new values of the physical constants of 1986, vapor pressure formulation based on the ITC-90, and psychrometer formulae, Zeitschrift für Meteorgie, 40: 340–344, 1990.

Swiatek, E: Derivation of Temperature (T_c) from the Sonic Virtual Temperature (T_s), Vapor Density (ρ_v)/Vapor Pressure (e) and Pressure (P), Campbell Scientific Inc., Logan, UT, USA, 1–5 pp., 2018.

Tanner, C. B. and Thurtell, G. W. Anemoclinometer measurements of Reynolds stress and heat transport in the atmospheric surface layer science lab, US Army Electronics Command, Atmospheric Sciences Laboratory, TR ECOM 66-G22-F. Page: R1-R10, 1969.

van Dijk, A.: Extension to 3D of "the effect of line averaging on scalar flux measurements with a sonic anemometer near the surface" by Kristensen and Fitzjarrald, Journal of atmospheric and Oceanic Technology, 19: 80–82, https://doi.org/10.1175/1520-0426(2002)019<0080:ETOTEO>2.0.CO;2, 2002.

Vaisala: Vaisala BAROCAP® Barometer PTB100 Series (User's Guide), M210839EN-A, 1–4. Helsinki, Finland, 2020.

Wallace, J. M. and Hobbs, P. V.: Atmospheric Science: An Introductory Survey, 2nd ed., Academic Press, Amsterdam, 350 pp., 2006.

Wang, X., Wang, C., Guo, Q., and Wang, J.: Improving the CO_2 storage measurements with a single profile system in a tall-dense-canopy temperate forest, Agricultural and Forest Meteorology, 228–229: 327–338, https://doi.org/10.1016/j.agrformet.2006.07.020, 2016.

Webb, E. K., Pearman, G. I., and Leuning, R.: Correction of flux measurements for density effects due to heat and water vapour transfer, Quarterly Journal of the Royal Meteorological Society, 106, 85–100, https//doi.org/10.1002/qj.49710644707, 1980.

Wilczak, J.M., Oncley, S.P., and Stage, S.A.: Sonic Anemometer tilt correction algorithm. Boundary-Layer Meteorology. 99: 127–150, https://doi.org/10.1023/A:1018966204465, 2001.

WMO: Guide to Instruments and Methods of Observation, WMO-No. 8, Volume I — Measurement of Meteorological Variables, World Meteorological Organization, Geneva, 548 p., 2018.

Wright, J. D., Johnson, A. N., and Moldover, M. R.: Design and Uncertainty for a PVTt Gas Flow Standard, Journal of Research of the National Institute of Standards and Technology, 108(1): 21–47, https://doi.org/10.6028/jres.108.00, 2003.

Wyngaard, J. C.: Spatial resolution of a resistance wire temperature sensor. The Physics of Fluids, 14: 2052-2054, https://doi.org/10.1063/1.1693718, 1971.

Yang, B., Hanson, P. J., Riggs, J. S., Pallardy, S. G., Heuer, M. H., Hosman, K. P., Meyers, T. P., Wullschleger, S. D., Gu, L. H.: Biases of CO_2 storage in eddy flux measurements in a forest pertinent to vertical configurations of a profile system and CO_2 density averaging, Journal of Geophysical Research, 112: D20123, https://doi.org/10.1029/2006JD008243, 2002.

Zhou, X., Gao, T., Pang, Y., Manhan, H., Li, X., Zheng, N., Suyker, A. E., Awada, T., and Zhu., J.: Based on atmospheric physics and ecological principle to assess the accuracies of field CO_2/H_2O measurements from infrared gas analyzers in closed-path eddy-covariance systems, Earth and Space Science, 8, e2021EA001763, https://doi.org/10.1029/2021EA001763, 2021.

Zhou, X., Yang, Q., Zhen, X., Li, Y., Hao, G., Shen., H., Gao, T., Sun, Y., Zheng, N.: Recovery of the 3-dimensional wind and sonic temperature data from a physically deformed sonic anemometer, Atmospheric Measurement Techniques, 11: 5981–6002, https://doi.org/10.5194/amt-11-5981-2018, 2018.